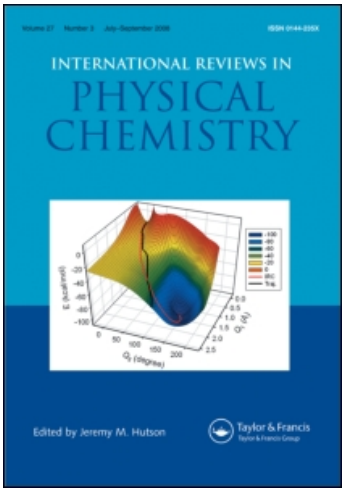

International Reviews in Physical Chemistry
Publication details, including instructions for authors and subscription information:
http://www.informaworld.com/smpp/title~content=t713724383

Vibrational relaxation in molecular crystals

Salvatore Califano[a]; Vincenzo Schettino[a]
[a] Department of Chemistry, University of Florence, Florence, Italy

To cite this Article Califano, Salvatore and Schettino, Vincenzo(1988) 'Vibrational relaxation in molecular crystals', International Reviews in Physical Chemistry, 7: 1, 19 — 57
To link to this Article: DOI: 10.1080/01442358809353204
URL: http://dx.doi.org/10.1080/01442358809353204

INTERNATIONAL REVIEWS IN PHYSICAL CHEMISTRY, 1988, VOL. 7, NO. 1, 19–57

Vibrational relaxation in molecular crystals†

by SALVATORE CALIFANO and VINCENZO SCHETTINO
Department of Chemistry, University of Florence,
Via Gino Capponi 9, 50121 Florence, Italy

The relaxation processes responsible for the finite lifetime of excited vibrational states in molecular crystals are discussed on the basis of recent experimental and theoretical developments. Experimental information on the lifetime of optically active phonons is obtained in the time domain by time-resolved CARS spectroscopy or in the frequency domain by high-resolution infrared and Raman spectroscopy. The experimental results are then interpreted in terms of many-body perturbation techniques or of molecular dynamics simulation.

The elementary mechanisms involved in vibrational energy relaxation processes are discussed in detail. These can be summarized as: (*a*) depopulation processes of phonon states via energy transfer to other phonon states; (*b*) pure dephasing processes due to interaction with thermal bath phonons; and (*c*) depopulation or scattering processes due to impurities and crystal defects.

The contributions to the phonon lifetime and band profile of these different mechanisms are analysed. The available experimental evidence is critically reviewed for lattice phonons and for internal vibrons in separate sections. For internal vibrons the specific case of the relaxation of two-phonon states is considered and different practical situations, ranging from the occurrence of sharp bound states outside the two-phonon continuum to the complete amalgamation of resonances in the continuum, are discussed.

1. Introduction

There are many elementary physical processes that occur on ultrashort time scales (10^{-9}–10^{-14} s). Among these are processes, including electronic and vibrational energy migration and relaxation, solvent relaxation, collisions in liquids, etc. that are of basic importance in chemical dynamics. Only recently direct experimental investigation of the dynamics of these molecular events has been made possible. With the advent of the laser a range of novel spectroscopic techniques has been developed, mainly based on the use of ultrashort light pulses, that has made the time evolution of these elementary processes directly observable. The purpose of the present review is to discuss the progress made in recent years in the understanding of the fundamental mechanisms that control the relaxation of vibrational excitations in molecular crystals toward equilibrium.

Vibrational excitations in crystals involve collective motions of the constitutitive entities, atoms or molecules. For molecular crystals it is convenient to distinguish between external (lattice) vibrations due to translational and librational motions of the molecules as a whole and internal vibrations due to the relative displacements of the atoms inside the molecules. For many molecular crystals a large frequency gap separates high-frequency internal from low-frequency lattice vibrations. However, some internal vibrations may fall into the same frequency range as the lattice modes, giving rise to crystal motions of mixed character. Crystal vibrations of true internal

† Dedicated to the late Professor Massimo Simonetta.

nature are often called *vibrons*, whereas lattice vibrations are called *phonons*. The term phonon is, however, utilized to indicate both lattice and internal vibrations whenever the distinction among them is not important.

The frequency and the eigenvectors of phonons in terms of molecular motions are normally obtained by diagonalization of the harmonic part of the crystal Hamiltonian (Califano *et al.* 1981). An enormous amount of work has been accumulated in the literature (Bonadeo and Burgos 1985) on the calculation of harmonic phonons and this has been of much help in the interpretation of the vibrational spectra of crystals and in the understanding of their dynamical behaviour. At the harmonic level, phonons are non-interacting independent crystal excitations with infinite lifetimes. Real phonons are, however, not independent of each other due to their interactions through high order anharmonic terms of the crystal Hamiltonian. These interactions are responsible for the relaxation of the phonon energy and thus for their finite lifetime.

In the context of solid-state spectroscopy the term relaxation is utilized to denote two different types of elementary processes which contribute to the randomization of the phonon energy in a crystal. The first concerns the simple loss of coherence of an ensemble of coherently excited molecules initially prepared by some appropriate non-linear optical pumping technique. Pure dephasing processes of this type are characterized, by analogy to spin relaxation theory, by a T_2' relaxation time. The second type of process represents instead the dissipation toward equilibrium of the energy initially accumulated in a given phonon state. To these energy decay or 'depopulation' processes is associated a T_1 relaxation time. The total relaxation time T_2 of a phonon state includes both contributions according to the equation

$$\frac{1}{T_2} = \frac{1}{2T_1} + \frac{1}{T_2'} \tag{1}$$

The two types of processes described above are intimately connected in the sense that all energy decay processes produce a loss of coherence of the excitation. The inverse is, however, not true since some specific phonon–phonon coupling mechanisms can destroy the coherence without altering the population of the excited state.

The interpretation of experimental data on phonon lifetimes requires a detailed knowledge of the phonon–phonon coupling terms of the Hamiltonian. Conversely the experimental determination of phonon lifetimes is of extreme importance for the study of anharmonic effects in solids.

Information on the relaxation of vibrational energy in crystals can be obtained by a variety of experimental techniques either in the time or in the frequency domain. These techniques are essentially spectroscopic and, therefore, concern only optically active phonons with zero wavevector. They have been critically discussed in recent reviews (Velsko and Hochstrasser 1985 a, Dlott 1986). The development of high-flux neutron sources and of high-resolution neutron spectrometers has made it possible to study relaxation processes also for $\mathbf{k} \neq 0$ phonons, by means of coherent inelastic neutron spectroscopy. To our knowledge this technique has been used in only one case (Dorner *et al.* 1982) so optical experiments remain for the moment the source of information on relaxation processes.

As far as spectroscopic measurements are concerned, the results of frequency domain experiments are obtained in the form of band profiles whereas those of time domain experiments furnish directly the phonon lifetime by recording the time decay of a suitable optical signal in the picosecond or in the nanosecond time scale. The two types of experiment are in principle equivalent, since the Fourier transform of the time

domain relaxation curve gives the band profile in the frequency domain. In some cases the relation between time and frequency domain experiments is particularly simple. A true exponential relaxation time T_2 corresponds to a homogeneously broadened Lorentzian band-profile with full width γ at half maximum (FWHM in units of cm^{-1})

$$\gamma = \frac{1}{\pi c T_2} \tag{2}$$

Relaxation processes cover a wide range of phonon lifetimes. As an example the lifetimes at 10 K of the lattice phonons of *l*-alanine (Kosik *et al.* 1984) are shown in table 1. In a relatively small frequency range these vary from a few picoseconds to more than 4 ns, showing that the efficiency of the relaxation processes may be completely different in the same crystal, even for closely related crystal modes.

Table 1. Lifetimes of *l*-alanine lattice phonons at 10 K.

$\omega(cm^{-1})$	Decay time
40	>4 ns
50	1·8 ns
75	550 ps
104	180 ps
105	120 ps
108	180 ps
121	18 ps
137	<10 ps

Phonon lifetimes or bandwidths are also extremely sensitive to temperature. The influence of temperature on the bandwidth and on the band frequency peak is easily detectable even at very low temperatures, as shown in figure 1 in the case of the $\omega_1(A_g)$ phonon of anthracene (Ouillon *et al.* 1984).

At very low temperatures ($T < 10$ K) typical low-frequency lattice phonons in aromatic crystals have, for instance, lifetimes from some hundred picoseconds up to several nanoseconds, corresponding to widths ranging from 0·1 to about 0·01 cm^{-1}. Well-isolated high-frequency vibrons in crystals made of small molecules may have longer lifetimes up to several hundred nanoseconds. As the temperature increases, phonon bands broaden and lifetimes shorten. At room temperature the same lattice phonons mentioned above have bandwidths of some centimetres^{-1}. This is due to the fact that relaxation processes involve both elastic and inelastic scattering with phonons of the thermal bath, whose population increases with temperature.

The theoretical interpretation of relaxation processes in molecular crystals is considerably simpler than for liquids or gases. In the case of solids the geometrical arrangement of the molecules is fixed and the composition of the thermal bath is well defined. For an ideal crystal it is possible to evaluate the relaxation mechanisms at the microscopic level if the intermolecular potential governing the dynamics of the system is known (Califano *et al.* 1981). Analytical forms of potential which reproduce the structure, the energy and the phonon dispersion curves of the crystal can be utilized to compute the high order phonon–phonon coupling terms of the hamiltonian and to evaluate the efficiency of the different relaxation channels. Calculations of this type have actually been made and are in progress in several laboratories. Real crystals present additional complications due to the occurrence of defects, dislocations and

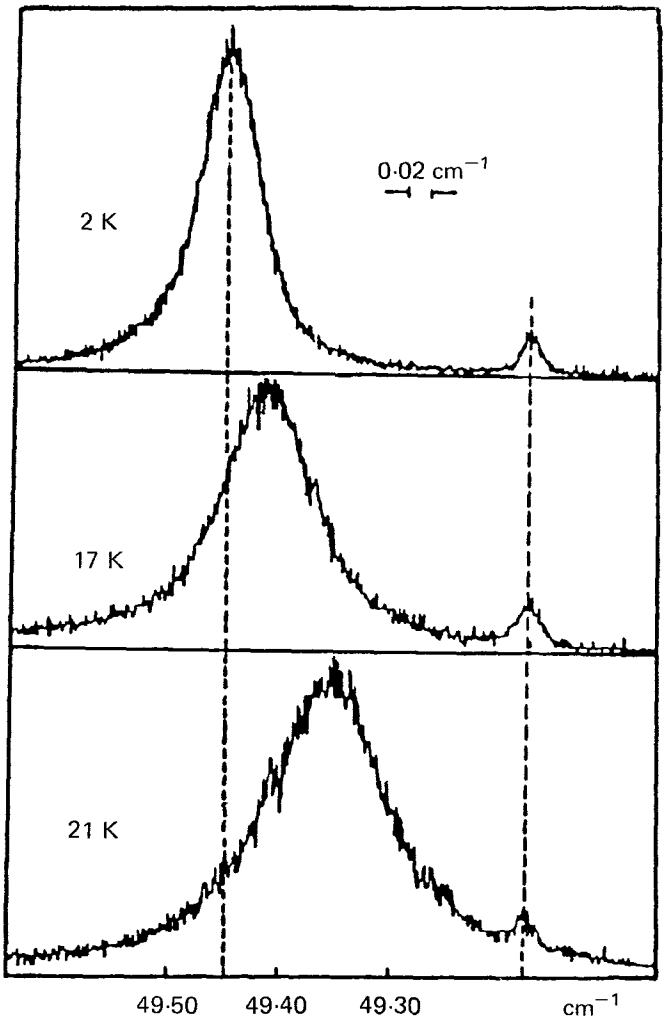

Figure 1. Band profile for the $\omega_1(A_g)$ phonon of anthracene at various temperatures.

isotopic impurities which can also dephase or trap the vibrational excitations. Owing to their random distribution in the crystal, stochastic methods are necessary to evaluate their contributions to the total relaxation time. In addition the elementary mechanisms by which they operate are not well known and often their influence can only be described by phenomenological approaches.

On the basis of the previous discussion, we can distinguish the following mechanisms of vibrational relaxation in molecular crystals:

(*a*) depopulation processes of a phonon state via energy transfer to other phonon states;
(*b*) pure dephasing processes due to the interaction with the thermal bath;
(*c*) depopulation processes via energy transfer to impurity levels; and
(*d*) dephasing processes due to scattering by impurities and defects.

In this review we discuss these different mechanisms on the basis of recent developments. In Section 2 the theory of anharmonic processes in molecular crystals is summarized and expressions for the relevant contributions to the phonon linewidths are presented. In Section 3 the experimental and theoretical results reported on individual molecular crystals are reviewed.

2. Theory of anharmonic processes

The anharmonic vibrations of a molecular crystal are normally treated by a perturbative expansion of the crystal hamiltonian in terms of phonon normal coordinates (Califano *et al.* 1981). Many-body perturbation techniques are used to evaluate anharmonic frequency shifts and bandwidths in connection with linear response theory to obtain the band profiles.

The perturbation expansion is reasonably carried out up to the fourth order with inclusion of quartic terms of the intermolecular potential. The treatment is appropriate for relatively small amplitudes of vibrations but runs into difficulties for large-amplitude motions such as those occurring at high temperatures or near phase transitions, especially in the case of order–disorder transitions.

For highly anharmonic systems alternative procedures have been developed. A convenient approach, widely used for plastic crystals, is based on the quaternion formalism (Walmsley 1986) first introduced by Hamilton in classical mechanics. A different treatment which eliminates the distinction between translational and rotational coordinates through the expansion of the potential in spherical harmonics has been proposed (Briels *et al.* 1985).

A technique, complementary to lattice dynamics discussed above, is that of molecular dynamics. Molecular dynamics is essentially a computer simulation of the dynamical evolution of a given ensemble of molecules. Since no perturbation expansion is used, the technique incorporates from the beginning the whole anharmonicity of the potential utilized. The method simply consists in solving the classical equations of motion for each molecule of the ensemble starting from an initial configuration and using analytical forms of interaction potential. By repeating the procedure at successive time steps one obtains a succession of system configurations which represent its time evolution. Short time steps, of the order of 0·01 ps, are necessary for precise solution of the equations of motion. The method furnishes directly space and time correlation functions of the dynamical variables whose Fourier transforms are the spectroscopic quantities of interest. Molecular dynamics is a purely classical method and thus the quantum statistics for bosons is not incorporated. Computed bandwidths thus converge to zero as $T \rightarrow 0$. On the other hand, at non-zero temperatures the full anharmonicity of the system is taken into account since no truncation of high-order terms is made as in the perturbative approach.

For the interpretation of relaxation times in normal crystals at moderately high temperatures, the perturbation expansion remains the chief approach since the different mechanisms of relaxation can be identified and their contribution evaluated separately. The perturbative techniques of solid-state theory (thermal Green's functions and hamiltonian renormalization) are presented in details in several papers and books. The specific case of molecular crystals is discussed in the book by Califano *et al.* (1981). Here we summarize the basic steps and the final results necessary for the interpretation of band profiles and relaxation times.

First the crystal potential is expanded in powers of the crystal normal coordinates

$$V = V_2 + V_3 + V_4 + \ldots = \frac{1}{2}\sum_{lm} C_{lm}Q_lQ_m + \frac{1}{3!}\sum_{lmn} C_{lmn}Q_lQ_mQ_n + \frac{1}{4!}\sum_{lmnp} C_{lmnp}Q_lQ_mQ_nQ_p + \ldots . \quad (3)$$

where l, m, n, p are composite indices comprehensive of the phonon branch label j and of the phonon wavevector label k. These will be specified whenever necessary. The C coefficients are derivatives of the potential with respect to normal coordinates, the generic derivative of order s being

$$C_{lmnp\ldots s} = \left(\frac{\partial^s V}{\partial Q_l \partial Q_m \ldots \partial Q_s}\right)_0 \delta(k_l + k_m + k_n + \ldots + k_s) \quad (4)$$

where the δ function assures the condition of momentum conservation.

The crystal hamiltonian then assumes the form

$$H = H_0 + H_1 + H_2 + \ldots \quad (5)$$

where $H_0 = T_0 + V_2$ is the zero-order hamiltonian which determines the dynamics of the system at the harmonic level, T_0 being the corresponding zero-order kinetic energy. H_1, H_2 etc. represent higher order terms of the hamiltonian which control the anharmonic phonon–phonon couplings. In the rigid body approximation the kinetic energy is quadratic in the normal coordinates or in the conjugate momenta. For non-rigid molecules this is not necessarily true and higher order terms appear in the kinetic energy, due to the fact that the inertia moments are coordinate-dependent for a non-rigid molecule. Higher terms of T are of the type (Walmsley 1985)

$$\left.\begin{aligned} T^{(1)} &= \sum_{lmn} \psi_{lmn} P_l Q_m P_n \\ T^{(2)} &= \sum_{lmnp} \psi_{lmnp} P_l Q_m Q_n P_p \end{aligned}\right\} \quad (6)$$

where the P are the conjugate momenta and the coefficients ψ_{lmn} and ψ_{lmnp} are not symmetric in the exchange of indices as are the terms of the potential expansion. These contributions are identically zero for linear and spherical-top molecules. Until now the contribution of $T^{(1)}$ and $T^{(2)}$ to the perturbation terms of the hamiltonian has been neglected.

By expressing the normal crystal coordinates in terms of phonon annihilation a and creation a^* operators

$$Q_l = \left[\frac{\hbar}{2\omega_l}\right]^{1/2} (a_l + a^*_{-l}) = \left[\frac{\hbar}{2\omega_l}\right]^{1/2} A_l \quad (7)$$

where the index -1 stands for reversal of k to $-k$ with the label j left unchanged, the terms of the crystal hamiltonian assume the form

$$\left.\begin{aligned} H_0 &= \sum_l \hbar\omega_l^0 (a_l^* a_l + \tfrac{1}{2}) = \sum_l \hbar\omega_l^0 (n_l + \tfrac{1}{2}) \\ H_1 &= \sum_{lmn} B_{lmn} A_l A_m A_n \\ H_2 &= \sum_{lmnp} B_{lmnp} A_l A_m A_n A_p \end{aligned}\right\} \quad (8)$$

where $\omega_l^0 = \omega_{jk}^0$ is the harmonic frequency of the phonon belonging to the j branch with wavevector $\mathbf{k}$ and n_l is the corresponding occupation number given by

$$n_l = [\exp(\hbar\omega_l/k_B T) - 1]^{-1} \tag{9}$$

The coefficients B are simply the C coefficients of equation (4) expressed in the space of the dimensionless operators A_l, that of order n being

$$B_{lmn\ldots s} = \frac{1}{n!}\left[\frac{\hbar^n}{2^n\omega_l\omega_m\ldots\omega_s}\right]^{1/2} C_{lmn\ldots s} \tag{10}$$

The B coefficients can be calculated to any order from analytical forms of the intermolecular potential once a suitable set of coordinates has been chosen to describe the $3N$ degrees of freedom of each molecule in the crystal. Details of these calculations are given in Califano *et al.* (1981).

By calculation of the self energy of the crystal by the thermal Green's function method or of the anharmonic phonon frequency by the hamiltonian renormalization procedure, one obtains the following result. The anharmonic phonon frequency is given, up to the fourth order, by

$$\omega_l = \omega_l^{(0)} + \omega_l^{(2)} + \omega_l^{(4)} \tag{11}$$

where $\omega_l^{(0)}$ is the harmonic frequency and $\omega_l^{(2)}$, $\omega_l^{(4)}$ are second- and fourth-order corrections to $\omega_l^{(0)}$, the first-order correction being equal to zero. These corrections are complex quantities of the form

$$\left.\begin{aligned}\omega_l^{(2)} &= \Delta_l^{(2)} + \mathrm{i}\Gamma_l^{(2)} \\ \omega_l^{(4)} &= \Delta_l^{(4)} + \mathrm{i}\Gamma_l^{(4)}\end{aligned}\right\} \tag{12}$$

where the real parts represent the contributions to the anharmonic frequency shift and the imaginary parts the contributions to the half bandwidth. For the interpretation of experimental data on relaxation processes the quantities of interest are essentially the half bandwidths Γ_l and only these will be considered in the following discussion. Detailed expressions for the anharmonic shifts are given by Kalus (1985) and Califano *et al.* (1981). Furthermore, since the experimental data concern optical phonons with zero wavevectors, we restrict ourselves to this case only.

From the perturbation treatment the full bandwidth $\gamma_l = 2\Gamma_l$ for an optical phonon ω_l in an ideal crystal is found to be the sum of several contributions, each arising from a specific depopulation or dephasing mechanism. For real crystals additional contributions arise from energy transfer to localized impurity levels and from scattering processes by defects, dislocations and impurities. In conclusion the bandwidth can be expressed in the form

$$\gamma_l = \gamma_l^{(3d)} + \gamma_l^{(4d)} + \gamma_l^{(3u)} + \gamma_l^{(4u)} + \gamma_l^{(4u)'} + \gamma_l^{(4dp)} + \gamma_l^{(4dp)'} + \gamma_l^{(i)} + \gamma_l^{(df)} \tag{13}$$

where the superscript specifies the relaxation mechanism and the number of phonons involved. In particular d stands for down-conversion, u for up-conversion, dp for dephasing, i for impurity and df for defect. We discuss these contributions separately.

2.1. *Depopulation mechanisms*

Processes of phonon state depopulation can be separated into down and up mechanisms, corresponding to transfer of the phonon energy to lower or higher energy phonons, respectively. The simplest second- and fourth-order processes are illustrated below.

Diagrams 1 and 2 describe three- and four-phonon down conversion processes, where an optical phonon ω_l decays into two (diagram 1) or three (diagram 2) lower frequency phonons.

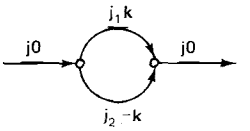

Diagram 1. Three-phonon down-conversion.

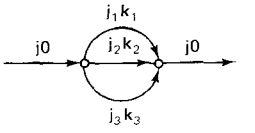

Diagram 2. Four-phonon down-conversion.

The contribution (Maradudin 1968, Califano *et al.* 1981, Kalus 1985) to the linewidth is, for diagram 1

$$\gamma_l^{(3d)} = 36\pi\hbar^{-2} \sum_{mn} |B_{lmn}|^2 (n_m + n_n + 1)\delta(\omega_l - \omega_m - \omega_n) \tag{14}$$

and for diagram 2 (Cowley 1963, 1965, Kalus 1985)

$$\gamma_l^{(4d)} = 192\pi\hbar^{-2} \sum_{mnp} |B_{lmnp}|^2 [(n_m + 1)(n_n + 1)(n_p + 1) - n_m n_n n_p] \times \delta(\omega_l - \omega_m - \omega_n - \omega_p) \tag{15}$$

Up conversion processes are represented in diagrams 3–5.

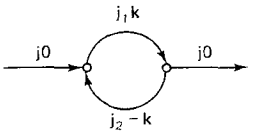

Diagram 3. Three-phonon up-conversion.

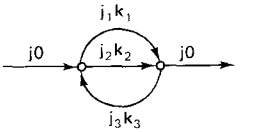

Diagram 4. Four-phonon up-conversion to a two-phonon state.

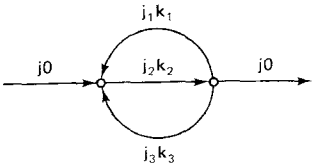

Diagram 5. Four-phonon up-conversion.

Diagram 3 describes a three-phonon process where the fusion of the optical phonon ω_l with a phonon ω_m produces a higher-energy phonon ω_n and its contribution to the linewidth is

$$\gamma_l^{(3u)} = 72\pi\hbar^{-2} \sum_{mn} |B_{lmn}|^2 (n_m - n_n)\delta(\omega_l + \omega_m - \omega_n) \tag{16}$$

In the fourth order diagram 4 the fusion of the ω_l and ω_m produces a two-phonon state, with contribution to the linewidth (Kalus 1985)

$$\gamma_l^{(4u)} = 576\pi\hbar^{-2} \sum_{mnp} |B_{lmnp}|^2 [n_m(n_n+1)(n_p+1) - (n_m+1)n_n n_p] \times \delta(\omega_l + \omega_m - \omega_n - \omega_p) \tag{17}$$

The last diagram 5 describes the fusion of ω_l with two phonons of the bath and its contribution to the linewidth is

$$\gamma_l^{(4u)} = -576\pi\hbar^{-2} \sum_{mnp} |B_{lmnp}|^2 [n_m(n_n+1)(n_p+1) - (n_m+1)n_n n_p] \times \delta(\omega_l - \omega_m + \omega_n + \omega_p) \tag{18}$$

This process is less probable than the others and it is likely to occur only at high temperatures when the thermal bath is strongly populated.

More complex fourth-order diagrams which also contribute to the bandwidth are shown below:

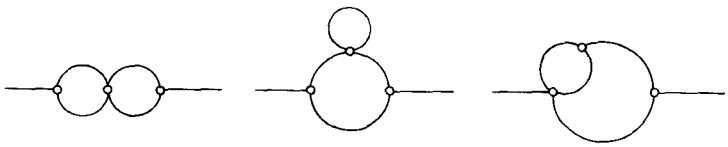

Diagram 6. Diagram 7. Diagram 8.

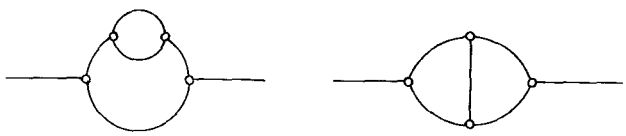

Diagram 9. Diagram 10.

For simplicity only one diagram, representative of the whole series of up and down processes is shown. Their contributions to the crystal self-energy has been discussed by Tripathi and Pathak (1974) and will not be reported here.

In all processes considered above, both energy and momentum are conserved. Energy conservation is ensured by the δ functions of equations (14)–(18) and momentum conservation is included in the expression of the B coefficients (see equation (4)).

Since three-phonon processes contribute to the second-order correction whereas four-phonon processes contribute to the fourth-order correction to the phonon frequency, the former are more probable than the latter. According to equations (14)–(18), the contribution of three-phonon processes (diagrams 1 and 3) is proportional to the first power of the phonon occupation numbers whereas that of four-phonon processes (diagrams 2, 4 and 5) depends upon products of two occupation numbers. Therefore in the classical limit ($\omega > k_B T/\hbar$), the former are proportional to T and the latter to T^2.

An important difference between down and up processes is their contribution to the low-temperature bandwidths. At $T \simeq 0$ all phonon occupation numbers are equal to zero and thus all up contributions vanish, since these require the thermal bath to be

populated. On the contrary, down contributions are still active at $T \simeq 0$ as shown by equations (14) and (15). For an ideal crystal therefore the residual bandwidth at very low temperature is a direct measure of the down contributions. For a real crystal the situation is more complex since decay processes into impurity levels are also active at $T \simeq 0$.

Since, as discussed in Section 2.2, pure dephasing processes are inactive when the thermal bath is not populated, the relaxation processes at $T \simeq 0$ can be separated into two contributions, one due to the down processes of type 14 and 15 and one due to impurity effects. The first results always in homogeneous broadening whereas the second may result in inhomogeneous broadening with a frequency spread Δ_i. We recall here that the Raman band profile is given by (Laubereau and Kaiser 1978)

$$I(\omega) = K \int dt \langle Q(0)Q(t) \rangle \exp(i\omega t) \tag{19}$$

where the correlation function $\langle Q(0)Q(t) \rangle$ can be expressed in the form

$$\langle Q(0)Q(t) \rangle = \exp[-(i\omega_0 + \gamma/2)t + \Delta_i^2 t^2/2] \tag{20}$$

ω_0 being the peak frequency and $\gamma = 1/2T_1$ the homogeneous width. We obtain the following results for Raman band shapes at very low temperature.

When Δ_i is negligible with respect to γ, i.e. when $\Delta/\gamma \ll 1$, a pure lorentzian profile is obtained. When the inhomogeneous broadening is large, i.e. when $\Delta/\gamma \gg 1$, the profile is gaussian. In intermediate cases a Voigt profile, which is the convolution of a gaussian and a lorentzian, is obtained.

All cases considered above are experimentally observed, although most observed Raman bands show a pure lorentzian profile. The lattice phonon band of anthracene (Ouillon *et al.* 1984) at 49·45 cm^{-1} of figure 2 is a typical example. In a few other cases, especially when a large number of impurities is present, gaussian and Voigt profiles have been observed.

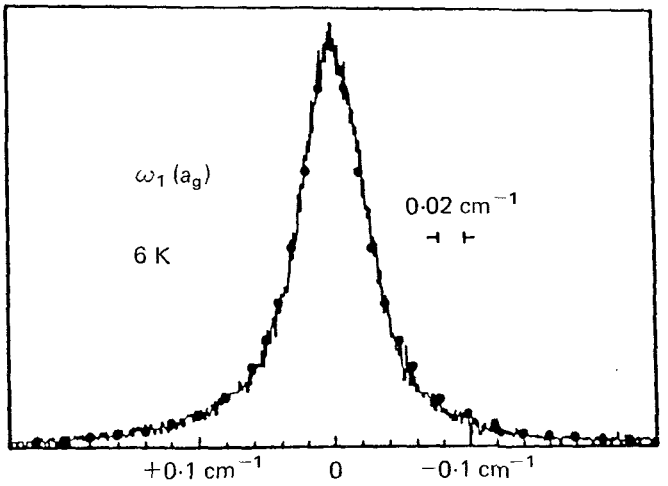

Figure 2. Experimental and convoluted lineshape of the $\omega_1(A_g)$ of anthracene at 6 K. Full line: experimental curve. Dots: convoluted Lorentzian curve.

At $T \simeq 0$, when all occupation numbers vanish, equation (14) assumes the simple form

$$\gamma_l^{(3d)}(0) = A \sum_{mn} |B_{lmn}|^2 \delta(\omega_l - \omega_m - \omega_n) \tag{21}$$

and, in the limit of constant coupling coefficients, the bandwidth is proportional to the two-phonon density of states (Della Valle *et al.* 1983).

2.2. *Pure dephasing processes*

Pure dephasing processes randomize the phase of the population of a phonon state without changing its occupation number. Processes of this type are due to both elastic and anelastic scattering with phonons of the thermal bath and are controlled by fourth or higher-order terms of the crystal hamiltonian.

The simplest elementary scattering process (Ouillon *et al.* 1984, Ivanov *et al.* 1966) leading to pure dephasing is represented by diagram 11 which is a special case of diagram 4 with $j_3 = j$ and $\mathbf{k}_3 = 0$.

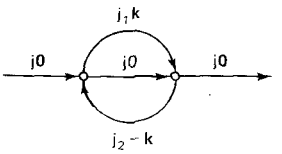

Diagram 11. Energy exchange dephasing process.

In this process two phonons $j_1\mathbf{k}$ and $j_2 - \mathbf{k}$ of the thermal bath exchange energy and this modulates the energy of the optical phonon $j\mathbf{0}$. Its contribution is easily found from equation (17) to be

$$\gamma_l^{(4dp)} = 576\pi\hbar^{-2} \sum_{mn} |B_{llm-n}|^2 n_n(n_m + 1)\delta(\omega_n - \omega_m) \tag{22}$$

Another pure dephasing process (Ouillon *et al.* 1984) arises from an elastic scattering between the optical phonon ω_l and a phonon ω_m of the thermal bath. This process, represented by diagram 12, gives no direct contribution to the bandwidth but produces an anharmonic frequency shift which, from second-order perturbation theory is

$$\Delta\omega_l = 12\hbar^{-1} B_{llm-m}(2n_m + 1) \tag{23}$$

At higher orders, however, the phonon ω_m is coupled to the thermal bath by a series of processes which cause its annihilation or creation. One of these processes is shown by diagram 13. These decay processes induce fluctuations in the occupation number n_m of equation (23) which in turn induce fluctuations in the anharmonic shift $\Delta\omega_l$.

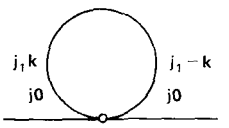

Diagram 12. Elastic scattering process.

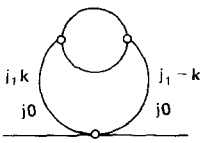

Diagram 13. Elastic scattering process coupled to the thermal bath.

This contribution has been discussed by several authors. A convenient approach is that of Harris *et al.* (1977) based on the stochastic fluctuation theory. According to these authors, each scattering process of the type shown in diagrams 12 and 13 involving a phonon ω_m ($m = j_1\mathbf{k}$) of the thermal bath with lifetime τ produces an effective shift

$$(\Delta\omega_l)_{\text{eff}} = \Delta\omega_l[1 + (\Delta\omega_l\tau)^2]^{-1} \exp[-\hbar\omega_m/k_BT] \tag{24}$$

which gives rise to the additional contribution to the bandwidth

$$\gamma_l^{(4dp)'} = \pi^{-1}\tau\Delta\omega_l(\Delta\omega_l)_{\text{eff}} \tag{25}$$

The same result has been obtained by Perrin (1987) using the Green's function formalism and considering the contribution to the self-energy of the infinite series of diagrams of the type shown in diagrams 11–13.

All pure dephasing processes require the thermal bath to be populated, as shown by equations (22)–(25) and are thus ineffective at very low temperature.

2.3. *Impurities and defects*

In real crystals the interpretation of experimental data on relaxation processes is complicated by the presence of impurities and static defects which give additional contributions to the bandwidths or decay times. Although these contributions cannot in general be separated one from the other, it is still convenient to discuss them separately, as they involve conceptually different mechanisms.

Most work on the subject concerns internal vibrons, these being similar to electronic excitons, so that theories developed for the latter can be easily adapted to cover the vibron situation. The effects are normally specific of each vibron state and thus it is more convenient to discuss them in detail in Section 3.2, where the relaxation of vibrons in individual molecular crystals is reviewed. Here we limit ourselves to the general aspects of the problem, discussing the two basic mechanisms, energy trapping and scattering processes, which influence the phonon lifetimes. Furthermore, our discussion will be limited to impurities, as isotopic impurities, normally present in molecular crystals. Mixed crystals, with large concentrations of impurities will not be treated.

2.3.1. *Energy trapping by impurities*

In molecular crystals the main impurities are represented by isotopic species present in natural abundance. These mass defects do not appreciably alter the intermolecular potential and thus have negligible influence on the collective low-frequency lattice phonons. In the case of high-frequency vibrons, however, they introduce new internal levels in the vibron manifold and may act as efficient energy traps, as long as the energy difference can be transferred to the thermal bath via acoustic phonons. In addition they can scatter the vibrons giving rise to dephasing.

For a relatively large mass difference, as in the case of deuterium impurities, the new level may fall outside the vibron band, as normally happens for internal modes dominated by hydrogen motions. In this case the impurity level can often be identified by standard spectroscopic techniques and its lifetime can be determined in much the same way as for other vibron levels. The few existing experimental data (Velsko and Hochstrasser 1985b, Ho *et al.* 1983, Trout *et al.* 1985, Chronister and Dlott 1983,

Chronister *et al.* 1985) show that the lifetime of the impurity of a light compound in a host lattice of the deutero compound is much longer than in the neat crystal and vice versa. This confirms the current idea that diluted impurity levels behave in many respects as well-localized excitations, i.e. as vibrations that the crystal cannot propagate.

For small mass defects, the impurity level falls inside the vibron band and the energy transfer process becomes near resonant. In this case the trap modes are almost completely driven by the collective motions of the host lattice and the same concept of the trap is lost. Such a situation is met for ^{13}C impurities in aromatic crystals. Time-resolved CARS experiments by Hochstrasser and his group (Trout *et al.* 1985) have shown large effects on some internal modes of benzene by adding 6·6% impurities of $^{13}CC_5H_6$ to pure $^{12}C_6H_6$. Whether the effect is due to a trapping or to a scattering process is difficult to judge. Abram and Hochstrasser (1980) have proposed a simple equation for the decay rate constant of a vibron in a mixed crystal, assuming that the overall population decay is a golden rule process controlled by anharmonic coupling among the internal modes at each site and the bath phonons. A detailed discussion of the trapping in mixed crystals is given in the review by Velsko and Hochstrasser (1985 a).

2.3.2. *Scattering by impurities and defects*

Both time and frequency domain experiments on phonon relaxation are very sensitive to crystal preparation, especially at low temperatures. Most of the simple organic compounds are liquid or gaseous at room temperature and extended concentration of defects and strains can be produced in the freezing process. These defects, together with impurities, introduce disorder in the crystal, break the translational symmetry and act as scattering centres for phonons and vibrons.

The theory of disorder in crystals is well established (Elliott *et al.* 1974) and is presented in compact form in a review by Elliott (1975). Using double-time Green's functions, it is possible, although not easy, to compute the density of states of the disordered crystal, to correlate it with the band shapes and to find the conditions for the appearance of local modes in the frequency spectrum.

For molecular crystals, Klafter and Jortner (1978) have treated the specific case in which the optical mode lies at the bottom of the density of states, a situation which is often encountered in practice (e.g. the ω_1 internal mode of CO_2). Although their treatment is devised for triplet exciton states, it is sufficiently general to be extended easily to vibrons. They use a simple second-order Anderson hamiltonian of the type

$$H_2 = \sum_n \Delta_n a_n^* a_n \tag{26}$$

where a_n^* and a_n are creation and annihilation operators for excitons on site n and Δ_n represents the deviation of the exciton energy from the mean value, due to structural disorder. Using the average t-matrix approximation (ATA) and assuming a gaussian distribution of local site excitation energies with a width D, they compute the self-energy of the disordered crystal and obtain for the band profile the expression

$$I(\omega) \simeq \frac{\pi D^2 \rho_0(\omega)}{[\hbar\omega + B - D^2 G^0_{nn}(\omega)]^2 + [\pi D^2 \rho_0(\omega)]^2} \tag{27}$$

where B is the half width of the exciton band, $\rho_0(\omega)$ the density of states of the ideal crystal and $G^0_{nn}(\omega)$ the corresponding Green's function. The theory predicts that for

$D > 2B$ the band is inhomogeneously broadened whereas for $D \ll 2B$ the band is motionally narrowed, i.e. is much narrower than the exciton band.

Abram and Hochstrasser (1980) discussed the effect of disorder in time domain experiments. According to them, theories developed in the frequency domain cannot be simply transposed to the time domain by Fourier transforming the equations, because of the approximations involved in the calculation of the Green's function of the disordered crystal. They developed the theory of coherence loss entirely in the time domain using the Anderson hamiltonian of equation (26), obtaining for the intensity decay of the CARS signal the expression

$$I_c = A \exp[(-t/\tau)^{1/2}] \tag{28}$$

where

$$\frac{1}{\tau} = \frac{2\pi}{h} D^2 \rho(\omega) \tag{29}$$

D^2 being the second moment of the Gaussian energy deviation Δ. This equation fits the experimental data well for the coherence decay of the internal vibron of $\alpha - N_2$ at 1·6 K with $\tau = 17$ ns.

3. Relaxation processes

In the previous section we discussed, in general terms population decay and pure dephasing processes controlling the lifetime of phonons and vibrons. In this section we discuss some specific cases in terms of these mechanisms.

By changing the molecular system, the particular phonon, vibron or vibron component, the experimental conditions (temperature, pressure, etc.) and the type and concentration of defects or impurities, a variety of structural and environmental situations can be probed systematically. Work has been collected in recent years on the dynamics of vibrational excitations in molecular crystals using stimulated Raman, CW or time-resolved CARS and spontaneous Raman techniques. This has been paralleled by theoretical efforts to calculate relaxation times from model potentials. Important matters like population decay contrasted to dephasing mechanisms, mode dependence of the decay rates, scattering or trapping at impurities and defects and finite temperature effects have been examined. Although a clear picture of the subject is far from having been obtained, the available experimental information may suggest possible trends of some particular issues or help in the planning of novel experiments to clarify the mechanisms of vibrational relaxation. A summary of the experimental results is discussed in the following for systems of increasing molecular complexity. The available information suggests that the general behaviour of lattice phonons and vibrons may be rather different. For this reason we discuss these subjects separately.

3.1. *Relaxation processes of lattice phonons*

3.1.1. *α-Nitrogen*

The lattice phonons of the α-form of crystalline N_2 have been studied extensively by neutron, Raman and infrared spectroscopy. This crystalline modification is cubic, space group T_h^6(Pa3) with four molecules per unit cell oriented along the four body diagonals of the cube. At the Γ point of the Brillouin zone ($\mathbf{k} = 0$), the 17 lattice modes

classify in the factor group symmetry as three Raman-active librational modes F_{g+}, F_{g-} and E_g, two infrared active modes F_{u+} and F_{u-} and two inactive modes E_u and A_u. The frequency of these lattice vibrations, determined by neutron spectroscopy (Kjems and Dolling 1975) at 15 K, are listed in table 2 together with the bandwidths of the three Raman and of the two infrared active modes. NQR measurements (Brookeman *et al.* 1970, 1971) have shown that large amplitude motions of the molecules take place even at very low temperature. A molecular dynamics simulation (Cardini and O'Shea 1985) has substantiated this finding, giving support to the idea that α-N_2 has an unusual anharmonic character. Comparison of the bandwidths (Anderson and Leroi 1966, Ron and Schnepp 1967, St Louis and Schnepp 1969) of table 2 with those measured for several other molecular crystals confirms the high anharmonicity of the lattice motions of α-N_2, since they are unusually large even in regions of low density of phonon states.

Several phenomenological or *ab initio* intermolecular potentials have been proposed (see Califano *et al.* 1981) to reproduce the experimental phonon frequencies of α-N_2. These cover a large variety of analytical forms, ranging from simple atom–atom to sophisticated anisotropic models with and without inclusion of electrostatic interactions between point charges or point quadrupoles located on the molecules. The large number of calculations performed at the harmonic level by standard lattice dynamics has been complemented by several anharmonic calculations of the phonon frequencies using manibody perturbation (Kobashi 1978), self-consistent (Raich *et al.* 1974) or mean-field (Antrygina *et al.* 1984), random phase approximation techniques (Jansen *et al.* 1984, Van der Avoird *et al.* 1984, Briels *et al.* 1984) and molecular dynamics (Cardini and O'Shea 1985). Only in three cases, however, was the anharmonic treatment extended to include a calculation of the relaxation processes.

A first attempt to explain the observed phonon band profiles in terms of anharmonic three-phonon decay processes was made by Kobashi (1978) who utilized a simple Lennard-Jones potential. Molecular dynamics simulation (Cardini and O'Shea 1985) showed that this potential is unable to reproduce the stability of the α-N_2 structure. More realistic intermolecular potentials, proposed by Berns and Van der Avoird (1980) and by Murthy *et al.* (1983) were utilized by Signorini *et al.* (1985) for the same type of calculations. The computed bandwidths are compared to experiment in table 2. The three calculations reported in this table, although made with different potentials, yield practically the same results. In agreement with experiment, large widths are computed for the broad F_{u+} and F_{g+} bands and small widths are obtained for the narrower F_{u-}, F_{g-} and E_g bands. In all cases, however, except for the E_g band, the computed width is larger than the experimental one, proving that the three

Table 2. Experimental and calculated bandwidths of α-N_2 lattice phonons in cm^{-1}.

	Exp. (15 K)		Calc. (0 K)		
	ω	γ	γ	γ	γ
F_{u+}	69	6	12·6	11·1	11·6
E_u	54	—	1·9	1·9	2·5
F_{u-}	48	0·5	1·3	1·2	2·5
A_u	47	—	0·7	1·0	1·1
F_{g-}	60	5	5·6	7·2	7·7
F_{g+}	36	0·8	1·3	1·2	1·3
E_g	33	0·8	1·0	0·6	0·6

potentials overestimate the phonon–phonon coupling coefficients. Whether or not this is due to a failure of the perturbative approach for crystals with large amplitude motions or simply to the inadequacy of the potentials is still open to discussion. Briels *et al.* (1984) have discussed the problems arising in lattice dynamics calculations because of the initial separation between translational and librational motions shared by all perturbative approaches. They have developed a new formalism for anharmonic calculations, the random phase approximation method (RPA), which eliminates this separation. Application of this technique to α-N_2 yields phonon frequencies in better agreement with the experimental data than those of previous authors. The method has not yet been extended to the calculation of bandwidths and thus it is difficult to discuss it in the framework of our subject.

The mechanisms of vibrational energy relaxation at 0 K have been discussed by Signorini *et al.* (1985) in terms of three-phonon down conversion processes. As discussed in the previous section up-conversion and pure dephasing processes are inactive at 0 K and thus only down-conversion processes contribute to the phonon relaxation for an ideal crystal. For each lattice phonon, a limited number of preferential decay channels exists, sometimes only one, because of the severe restrictions imposed by energy and momentum conservation relations. In the paper by Signorini *et al.* (1985) the effective decay channels are calculated and visualized in two-dimensional plots showing the two-phonon density of states and the corresponding contributions to the down processes, respectively. Comparison of the two plots shows that the contributions to the decay processes follow the pattern of the two-phonon density of states except in the very low frequency region where additional peaks appear.

3.1.2. *Carbon dioxide*

The crystal structure of solid CO_2 is the same as that of N_2. The crystal is cubic, space group Pa3(T_h^6), with four molecules per unit cell oriented along the body diagonals of the cube and possesses 17 $\mathbf{k}=0$ lattice modes, three Raman active ($2T_g + E_g$), two infrared active ($2T_u$) and two modes inactive in both spectra ($E_u + A_u$). In contrast to crystalline nitrogen, the anharmonicity of solid CO_2 is very low. The study of phonon relaxation processes is thus of special interest in this case since perturbative approaches are expected to work well and anharmonic calculations are representative of the validity of the model potential adopted.

Extensive work on the dynamical properties of crystalline CO_2 has been performed by Schmidt and Daniels (1980) who studied under low resolution (about 1 cm^{-1}) the variation with temperature of the constant volume bandwidths of all three Raman active modes. The resolution is sufficient for the broad T_{g+} band at 134 cm^{-1} but inadequate for the very narrow low frequency bands at 93·3 (T_{g-}) and 74·8 (E_g) cm^{-1}. Recently the constant pressure width of these two bands has been measured as a function of temperature between 6 and 70 K by Ranson *et al.* (1988) under very high resolution (0·005 cm^{-1}).

The contribution of three-phonon decay processes to the bandwidth of the lattice modes has been evaluated by Procacci *et al.* (1987). They found that the best available intermolecular potential for CO_2, which reproduces correctly the energy, the structure, the lattice frequencies and even the single phonon Gruneisen parameters, predicts bandwidths about 10 times larger than the experimental ones. They produced a new intermolecular potential which includes reparameterized atom–atom potentials and

Table 3. Experimental and calculated frequencies and bandwidths of the CO_2 lattice phonons (5 K) in cm^{-1}.

Symm.	ω_{exp}	ω_{calc}	γ_{exp}	γ_{calc}§
T_{g+}	135·1	135·9	1·5†	1·7
T_{g-}	93·3	87·0	0·24‡	0·22
E_g	74·8	74·9	0·12‡	0·16
T_{u+}	114·5	118·4	—	2·6
A_u	106·4	103·3	—	0·82
E_u	95·4	92·4	—	0·47
T_{u-}	66·7	75·2	—	0·18

† Schmidt and Daniels (1980).
‡ Ranson *et al.* (1987).
§ Procacci *et al.* (1987).

electrostatic interactions described by a complex charge distribution in the molecule. Calculated bandwidths at 5 K agree well with experiments as shown in table 3.

The calculated variation with temperature of the bandwidth is compared with experimental results in figure 3. In the case of the high frequency T_{g+} and T_{g-} phonons, the experimental data agree well with calculations, showing a linear T dependence in

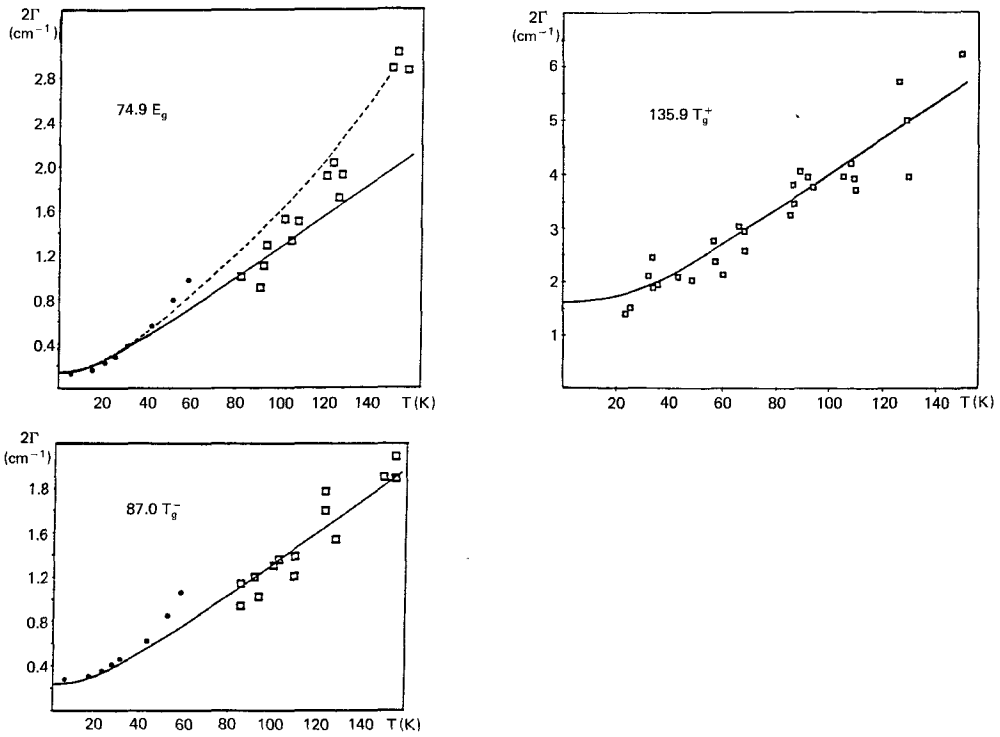

Figure 3. Temperature dependence of the linewidth of the lattice phonons of CO_2. Dots: experimental data at constant pressure (Ranson *et al.* 1988); squares: experimental data at constant volume (Schmidt and Daniels 1980); solid line: calculated curves for three phonon processes; dashed line: calculated curve for three and four-phonon processes (Procacci *et al.* 1987).

the classical limit, characteristic of three-phonon processes. In the case of the lowest energy phonon E_g the calculated curve fits the experimental data only up to about 40 K. Above this temperature the experimental points lie systematically above the calculated curve and show a clear T^2 dependence which proves that higher order relaxation processes are also active.

To explain the T^2 dependence of the width of the E_g phonon, Schmidt and Daniels (1980) have proposed a four-phonon process in which the E_g phonon decays into three acoustic phonons of one-third frequency. From equation (15), putting $n_m = n_n = n_p = n$, one obtains

$$\gamma = b[(n+1/2)^2 + 1/12] \tag{30}$$

This equation reproduces the experimental data and, according to the calculated dispersion curves of Procacci *et al.* (1987), the decay process $\omega = 3(\omega/3)$ is physically reasonable. This suggests that for very low anharmonicity, quartic terms of the potential may dominate the high temperature decay process.

3.1.3. *Naphthalene*

Naphthalene is one of the most studied molecular crystals both experimentally and theoretically. Crystalline naphthalene is monoclinic, space group $P2_1/c$ (C_{2h}^5) with two molecules per unit cell located on C_i sites. It possesses nine optically active lattice phonons, six active in the Raman ($3A_g + 3B_g$) and three in the infrared ($2A_u + B_u$). Experimental studies on phonon band profiles and lifetimes are limited to the Raman active phonons, which occur in the spectrum in the form of three doublets, each made of one A_g and one B_g mode. The experimental data are collected in table 4.

A pioneering study of the bandshape of the Raman active phonons is due to Bellows and Prasad (1979) who investigated the temperature dependence of the bandwidth of

Table 4. Experimental and calculated bandwidths of naphthalene lattice phonons at 0 K in cm^{-1}.

	$\omega_{exp.}$	$\gamma_{exp.}$			$\gamma_{calc.}$
	†	‡	§	¶	‖
ω_1	68	<0·05	0·05	0·038	0·06
ω_2	89	—	—	—	1·5
ω_3	121	1·3	—	—	2·3
ω_4	57	<0·05	0·035	0·024	0·04
ω_5	83	—	—	—	2·3
ω_6	141	1·4	—	—	2·6
ω_7	57	—	—	—	0·27
ω_8	108	—	—	—	2·0
ω_9	79	—	—	—	0·7

† Natkaniec *et al.* (1980).
‡ Bellows and Prasad (1979).
§ Ranson *et al.* (1984).
¶ Duppen *et al.* (1981).
‖ Della Valle *et al.* (1983).

the two lowest and of the two highest frequency phonons in the temperature range 2–300 K by means of conventional Raman spectroscopy. The study was limited to these four phonons since the two components of the central doublet at 83 and 89 cm^{-1} overlap almost completely already at 140 K because of thermal broadening, so that their evolution with temperature cannot be studied meaningfully. The two highest frequency phonons ω_3 and ω_6 have relatively large widths at 2 K and are thus conveniently studied by conventional Raman spectroscopy with a typical limiting resolution of about 0·3 cm^{-1}. The two lowest frequency phonons ω_1 and ω_4 have widths at 2 K which are about 100 times narrower. For this reason these authors were able to furnish only an upper limit of 0·05 cm^{-1} for the width of these two phonons. As the temperature increases the bands broaden and shift towards lower frequency.

The temperature evolution of the bandwidth of ω_1 and ω_4 obtained by Bellows and Prasad (1979) is shown in figure 4. They interpreted their results in terms of three-phonon decay processes and found that the experimental data were best fitted assuming only one down and one up process for ω_1 and ω_4 and two down processes for ω_3 and ω_6. The proposed decay processes are shown below:

$$\omega_1(A_g) \rightarrow [2(\omega_1/2)] + 7{\cdot}5(87-30)\,cm^{-1}$$

$$\omega_4(B_g) \rightarrow [2(\omega_4/2)] + 6{\cdot}5(98-30)\,cm^{-1}$$

$$\omega_3(A_g) \rightarrow 0{\cdot}6[2(\omega_3/2)] + 0{\cdot}4(91+30)\,cm^{-1}$$

$$\omega_6(B_g) \rightarrow 0{\cdot}5[2(\omega_6/2)] + 0{\cdot}5(111+30)\,cm^{-1}$$

In all cases therefore a dominant process is found to be the fission of the phonon into two phonons of half frequency. In addition, the up process is found to be about seven times more efficient than the down one for both ω_1 and ω_3.

More precise measurements of the bandwidths of ω_1 and ω_4 were performed by Duppen *et al.* (1981) (see table 4) by picosecond CARS spectroscopy. They measured the low temperature width of ω_1 and the temperature evolution of ω_4 between 2 and 60 K. Their interpretation of the relaxation processes is similar to that of Bellows and Prasad although a larger efficiency (about 20 times) is assigned to the up process. The variation with temperature of the lifetime of the ω_1 phonon in the range 1·5–70 K was subsequently determined by Schosser and Dlott (1984) who also studied the corresponding mode in naphthalene-d_8.

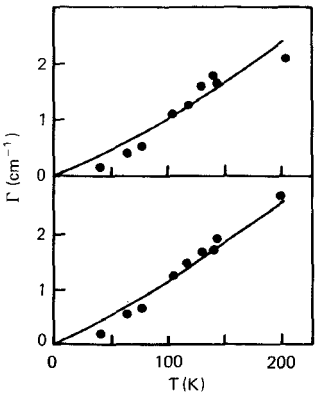

Figure 4. Temperature evolution of the linewidths of the ω_1 (*a*) and ω_4 (*b*) lattice phonons of naphthalene.

More recently, the low temperature width of ω_1 and ω_4 was measured by high-resolution Raman spectroscopy by Ranson *et al.* (1984) using a tandem Fabry–Perot interferometer–Raman spectrometer with a resolution of 0·02 cm^{-1}. The results are consistent with those obtained by ps CARS and are shown in table 4.

Detailed calculations of three-phonon decay processes in crystalline naphthalene have been made by Della Valle *et al.* (1983) using an analytical form of intermolecular potential which includes atom–atom and quadrupole–quadrupole interactions. The calculated widths, reported in table 4, are consistent with the experimental finding that ω_6 has a larger width than ω_3 and that both are much larger than ω_1 and ω_4. The calculated widths are in close agreement with experiment in the case of ω_1 and ω_4 but are larger by a factor of 2 than the experimental ones for the two highest Raman frequencies. With the same intermolecular potential these authors have calculated the most efficient decay channels. The calculations confirm that a preferential pathway for the decay is always the fission into two phonons of half frequency as proposed by Bellows and Prasad. They found, however, that depending upon the pattern of the dispersion curves, other decay processes are also important. The same conclusions were reached by Dlott and coworkers.

As discussed in section 2, phonon relaxation processes depend on the number of accessible decay pathways controlled by the numerical value of the B coupling coefficients. Assuming that the B coefficients are approximately the same, one obtains from equation (13) that the bandwidth is directly proportional to the two-phonon sum density of states defined as

$$\rho_{\text{sum}}[\omega_j(\mathbf{0})] = \sum_{kmn} \delta(\omega_j(\mathbf{0}) - \omega_m(\mathbf{k}) - \omega_n(-\mathbf{k})) \tag{31}$$

with zero total wavevector. This approximation works well, not only in the present case, but in nearly all the cases examined so far. Figure 5 shows the two-phonon sum density of states in the region of the lattice phonons of naphthalene together with the phonon widths, represented by vertical lines proportional in height to their numerical value.

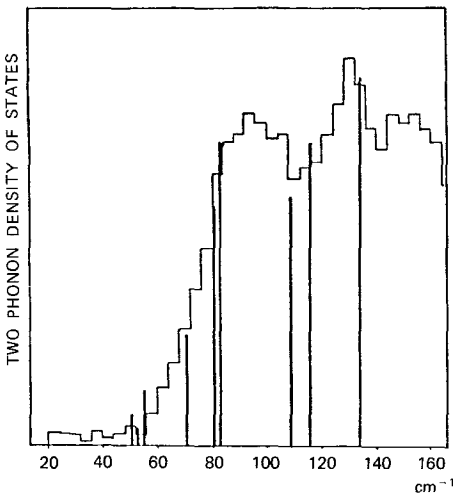

Figure 5. Two-phonon density of states of naphthalene. The vertical lines are proportional in height to the phonon linewidths.

Calculations of the width of the lattice phonons of naphthalene-d_8 have been made by Jindal and Kalus (1983) using three-phonon decay processes and agree well with the few available data.

3.1.4. *Anthracene*

Anthracene is another molecular crystal whose dynamical properties have been investigated widely. It crystallizes in the $P2_1/a$ (C_{2h}^5) space group with two molecules per unit cell on C_i sites and possesses nine lattice modes, six Raman active ($3A_g + 3B_g$) and three infrared active ($2A_u + B_u$).

Information on phonon relaxation processes are limited, as in the case of naphthalene, to the four out of the six Raman active bands which have sufficiently long lifetimes to be easily interpreted. The lifetime of the lowest frequency Raman phonon $\omega_1(A_g)$ at 49·45 cm^{-1} has been measured by Schosser and Dlott (1984) by picosecond CARS in the range 10–45 K. Ouillon *et al.* (1984) studied the evolution with temperature of the bandwidth of the four lowest frequency phonons $\omega_1(A_g)$, $\omega_6(B_g)$, $\omega_7(B_g)$ and $\omega_2(A_g)$ in the range 2–70 K by high resolution (0·02 cm^{-1}) Raman spectroscopy. Both groups of authors have interpreted the experimental data in terms of three-phonon processes. A single down and a single up process are sufficient to reproduce correctly the widths in the temperature range studied. In particular the dominant down process was suggested to be the decay into two acoustic phonons at half frequency for $\omega_1(A_g)$, $\omega_6(B_g)$ and $\omega_7(B_g)$. In the case of the higher energy phonon $\omega_2(A_g)$ the proposed decay process involves one acoustic and one optical phonon. These processes, together with the up process and the corresponding coupling coefficients are listed below in cm^{-1}:

ω	Down process	Up process	Coupling coefficient
A_g 49·45	2 × 24·72	(98·45–49)	1·0 cm^{-1}
B_g 57·50	2 × 28·75	(108·50–51)	1·1 cm^{-1}
B_g 71·20	2 × 35·60	(120·20–49)	0·78 cm^{-1}
A_g 82·40	57·50 + 24·90	(138·40–56)	1·0 cm^{-1}

The calculated curves of $\gamma^{(3d)}$ (curve a) and $\gamma^{(3u)}$ (curve b) as a function of temperature in the range 2–70 K are shown in figure 6 together with the experimental data. The curve c of figure 6 which fits the experimental data is the sum of curves a and b.

As in the case of naphthalene the widths of the lattice phonons follow exactly the pattern of the two-phonon density of states with zero total wavevector.

3.1.5. *Amino acids and peptides*

The lifetime of about 60 lattice phonons in eight of the simplest amino acids and peptides has been measured at low temperature by Kosic *et al.* (1983, 1984) by picosecond CARS. For about 50 phonons in these crystals they found exponential decay of the CARS signal and in only a limited number of cases was a different behaviour found. For phonons with exponential decay they conclude that only population relaxation mechanisms are active. For the others they assume that the observed inhomogeneous broadening is due either to impurities or to static disorder.

The picosecond CARS spectra of these compounds show some interesting features. In the case of the four amino acids studied (*l*-alanine, α-glycine, glutamic acid.HCl and *l*-histidine.HCl.H_2O) the lowest frequency phonons, occurring below 50 cm^{-1}, have

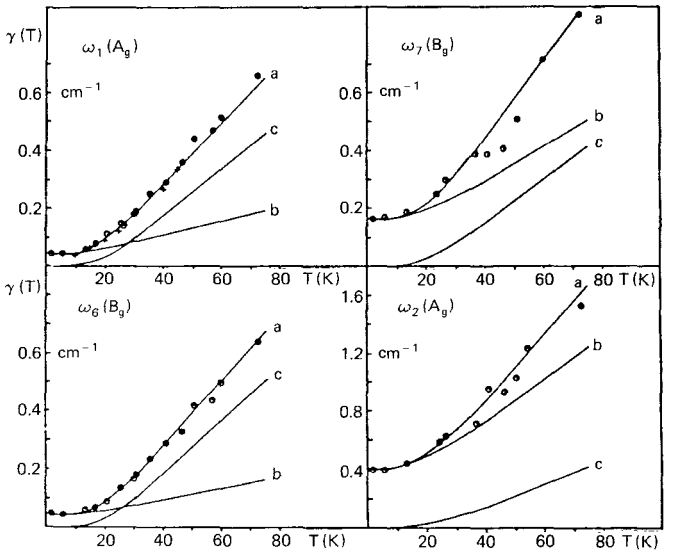

Figure 6. Temperature evolution of the linewidths of four lattice phonons of anthracene. Curve b: calculated contribution for down processes; curve c: calculated contribution for up processes; curve a: b + c. Dots and circles are experimental data.

unusually long lifetimes, of the order of nanoseconds. To our knowledge these are the longest lifetime lattice phonons known. In the case of the peptides (glycylglycine, *l*-alanyl-*l*-tyrosine.3H_2O, *N*-acetylglycine) and of acetanilide, low-frequency phonons have lifetimes comparable to those observed in normal Van der Waals crystals.

In these crystals the phonon lifetime decreases very rapidly as the phonon fequency increases. A typical example is that of *l*-alanine shown in table 1. The lowest phonon at 40 cm^{-1} has a lifetime longer than 4 ns whereas for phonons above 120 cm^{-1} the lifetime drops to less than 10 ps. Kosic *et al.* (1984) found that in all these crystals the phonon relaxation times follow a Ω^{-4} low, except for *l*-alanyl-*l*-tyrosine.3H_2O in which they obey a Ω^{-2} low. The Ω^{-4} behaviour is interpreted by them as due to a dominant decay process into two acoustic phonons of the same frequency whereas the Ω^{-2} dependence is assumed to be representative of decay processes into one acoustic and one optical phonon.

Ranson *et al.* (1985) have studied under high resolution (0·005 cm^{-1}) the variation of the bandwidth of the three lowest frequency phonons of α-glycine at 56, 73 and 79 cm^{-1} in the range 5–50 K and found that the experimental curves are perfectly fitted by one down three-phonon process into two acoustic phonons of the same frequency and one or two up processes, according to the decay equations

$$55{\cdot}95 \text{ phonon: } \omega_1 = 28;\ \omega_2 = 25;\ \omega_3 = 105;\ \omega_4 = 81;\ \omega_5 = 161 \text{ cm}^{-1}$$
$$\gamma(T) = 0{\cdot}004(1 + 2n_1) + 0{\cdot}05(n_2 - n_3) + 6(n_4 - n_5)$$

$$73{\cdot}05 \text{ phonon: } \omega_1 = 36{\cdot}5;\ \omega_2 = 25;\ \omega_3 = 83;\ \omega_4 = 98;\ \omega_5 = 156 \text{ cm}^{-1}$$
$$\gamma(T) = 0{\cdot}004(1 + 2n_1) + 0{\cdot}04(n_2 - n_3) + 2{\cdot}5(n_4 - n_5)$$

$$78{\cdot}65 \text{ phonon: } \omega_1 = 39;\ \omega_2 = 80;\ \omega_3 = 158{\cdot}65 \text{ cm}^{-1}$$
$$\gamma(T) = 0{\cdot}005(1 + 2n_1) + 1{\cdot}75(n_2 - n_3)$$

3.1.6. *Other crystals*

In addition to the crystals discussed above some few other crystals have been investigated. Calculations of phonon lifetimes have been made for crystalline ammonia (Della Valle *et al.* 1979) and high-resolution Raman measurements have been reported for tetracyanoethylene (Ranson *et al.* 1985). In addition, Prasad and Smith (1979) investigated some lattice phonons in *p*-bromochlorobenzene and in *p*-dichlorobenzene by conventional Raman spectroscopy and De Silvestri *et al.* (1985) studied by femtosecond spectroscopy the dephasing of some α-perylene phonons.

3.2. *Relaxation processes of internal vibrons*

3.2.1. *Diatomics*

The only crystals of diatomics that have been studied so far are α-N_2 and H_2 at low temperatures. A coherent excitation was produced by stimulated Raman (Abram *et al.* 1977, 1979) or stimulated Raman gain (Abram *et al.* 1980) and the vibrational exciton coherence loss was probed through the delayed coherent anti-stokes signal from the excited state.

The frequency of the vibrational excitation in N_2 (2346 cm^{-1}) and in H_2 (4165 cm^{-1}) is many times larger than the highest phonon frequency. Thus depopulation of the excited state by phonon emission is a high-order process of negligible importance in these cases. The only route for the depopulation is the trapping at isotopic impurities. These diatomics are ideally suited to investigate the role of intraband scattering, trapping and scattering at defects or impurity sites.

The coherence loss in α-N_2 has been found to be non-exponential with a time constant $T_2/2$ increasing from 1 ns to 14·5 ns in the first 100 ns of delay at 4 K. The decay is also found to be temperature-independent in the range 1·33 to 4 K. Contributions to the coherence loss from intraband scattering can thus be ruled out. In fact the exciton band has a width $W = 1{\cdot}5\ cm^{-1}$ and the A_g component probed in the experiment lies at the bottom of the exciton band. Thus intraband scattering would involve absorption of acoustic phonons of very low energy and such a process should be very sensitive to temperatures in the range investigated. The vibrational frequency of the major isotopic impurity ($^{14}N^{15}N$ with 0·74% natural abundance) occurs 40 cm^{-1} below that of the pure crystal. The trapping or scattering efficiency of the isotopic impurity in this case has been estimated to be very low and to cause decay times larger than experiment by two orders of magnitude. To probe the efficiency of scattering or trapping at impurities, experiments have been performed on samples with 10% of added $^{15}N_2$ with frequency 78 cm^{-1} below that of the pure crystal. The decay curves were found to be insensitive to the addition of isotopic impurities. From this data and by exclusion it was argued that the coherence loss in α-N_2 crystal is due to structural disorder. This is strongly suggested by the observation that the decay curve depends on sample preparation in the first 10 ns of decay. The presence of defects leads to local strain and thus to a distribution of site energies. The exact nature or distribution of the defects is not known but from the width of the $^{15}N_2$ impurity band it can be estimated that the width of the inhomogeneous distributions D has an upper limit of 0·025 cm^{-1}. The width of the inhomogeneous distribution is thus much smaller than the exciton bandwidth $D \ll W$. An approximate theory of exciton band shapes in disordered crystals with site diagonal disorder having a gaussian shape with variance D^2 has been discussed by Klafter and Jortner (1978) and leads to expression 27 for the band shape. In the present case the A_g exciton is in a place of the exciton band where the density of states

approaches zero and therefore equation (27) predicts a linewidth much smaller than D, as observed experimentally. The Fourier transform of the line shape 27 gives decay curves that slow down at high delay times in qualitative agreement with experiment. Better quantitative agreement with the α-N_2 experiment was obtained by Abram and Hochstrasser (1980) discussing the coherence loss directly in the time domain. The important point raised by these authors is that the exciton coherence decay will strongly depend on the position of $\mathbf{k}=0$ accessible states within the exciton band. When the $\mathbf{k}=0$ state is located at a singular point in the density of states, the decay will be strongly non-exponential. This is the case for the A_g exciton in α-N_2 for which $\rho(\omega^{A_g})\simeq 0$. If the $\mathbf{k}=0$ states fall in a high density region of the exciton band, the decay can be exponential. This is expected for the F_g state in α-N_2 although it has not been confirmed experimentally.

There are important implications of the α-N_2 results in connection with the discussion of coherence decay in crystals of larger molecules with complicated band structure. The scattering at defects and the scattering or trapping at isotopic impurities in α-N_2 has been found to contribute decay times in the range of several nanoseconds. If so, these processes are negligible in many cases since vibrational decay times in molecular crystals are generally in the range of a few picoseconds. It is, however, known that in α-N_2 the isotopic impurities fall in the well-separated band limit, and the effect in the amalgamated regime can be quite different. The implication of equation (27) is that the inhomogeneous broadening can be neglected when the exciton bandwidth is larger than the inhomogeneous distribution, $D/W\ll 1$. This condition is met for many vibrational modes in molecular crystals at low temperature. This motional narrowing effect arises from the competition between the correlation due to intermolecular interaction and the distribution of site energies. This points to the importance of explicitly considering vibrational excitations in the crystal as delocalized collective modes of the system. From this point of view, the position of the states under investigation within the exciton band always plays an important role.

The coherence loss in crystalline hydrogen has been studied for samples of p-H_2 with varying amounts of o-H_2 (Abram *et al.* 1980). The coherent amplitude decay is non-exponential and slows down at large delays. At 4·2 K the characteristic decay times in the initial stages range from approximately 25–6 ns for o-H_2 concentrations from 0·22% to 2·7%. In addition, the decay curves are found to be insensitive to temperature in the range 2–4·2 K. In p-H_2 the vibrational exciton has a bandwidth $W=4\,\mathrm{cm}^{-1}$ and the symmetric exciton component investigated lies at the bottom of the band. The vibrational frequency of o-H_2 impurities is 3–6 cm^{-1} below the $k=0$ exciton frequency of pure p-H_2. The temperature independence of the decay rules out intra-band scattering and trapping at the o-H_2 sites as possible sources of coherence decay. The observed decay must be ascribed to scattering at the impurity sites. The increase in concentration increases the number of scattering centres and thus the decay rates. Exciton scattering by a single impurity depends on the energy separation Δ between the impurity and the pure crystal levels, and on the value of Δ relative to the exciton bandwidth W. In the amalgamation limit ($\Delta<W$) the conclusions of the theories of scattering at defects are still valid. The situation in the separated band limit has been discussed by Velsko and Hochstrasser (1985b) who have shown that at low concentration C_B of impurities, the results of scattering by defects can be recovered with the assumption $D^2=C_AC_BW^2$. However, this model only gives a qualitative agreement with experiments in p-H_2. This can be ascribed to the fact that the o-H_2 impurities are not really in the separated band limit.

In conclusion, experiments for the N_2 and H_2 crystals give information on dephasing of the coherence amplitude of the vibrational exciton since population relaxation processes occur with much longer characteristic times. In fact, the vibron lifetime in crystalline natural H_2 at the triple point (13·6 K) has been measured (Delalande and Gale 1977) by stimulated Raman excitation and infrared detection of the collision-induced infrared fluorescence. A lifetime of 7·5 μs was obtained. For nitrogen the vibrational relaxation time in the liquid has been found to be 10^{11} times larger than the dephasing time (Calaway and Ewing 1975). The situation is quite different in crystals of polyatomic molecules.

3.2.2. *Benzene*

The dynamics of the vibrational excitons in the benzene crystal at 4 K have been investigated by high resolution and time-resolved CARS (Ho *et al.* 1981, 1983, Velsko *et al.* 1983, Trout *et al.* 1985). Experiments have been carried out on natural samples with 6% abundance of the isotopic species and on ^{12}C enriched samples with 0·15% residual isotopic impurity concentration (Trout *et al.* 1985). The relevant results on the decay times are reported in table 5 where some additional spectroscopic information relevant to the following discussion is also collected. The major points emerging from the benzene work are summarized below.

(*a*) The vibrational decay of the 991 cm^{-1} ring breathing mode has been studied by both picosecond and high-resolution CARS. The reciprocal of the linewidth obtained from the latter compares well with the decay time determined from the former technique, showing that time and frequency domain experiments give equivalent information.

Table 5. Vibrational relaxation times of fundamental modes in natural and isotopically pure benzene crystal at 4 K.

Mode	Symm.	^{13}C shift (cm^{-1}) †	Vibron bandwidth (cm^{-1}) ‡	§	¶	Pure crystal ω	Pure crystal $T_2/2$	Natural crystal ω	Natural crystal $T_2/2$	N. accept channels	$1/T_2$ (arb. units)
ω_6	e_{2g}	2	6	3	5	606	2650	606	94·7	0	0
ω_{10}	e_{1g}	1	12	21	23	854	884	854	379	0 1	0·1
ω_1	a_g	9	0	2		991 991·6	61·7 56	— —	39·2 35·6	2	1
ω_5	b_{2g}	4	0	17		—	—	1012	8	2	
ω_9	e_{2g}	2	13	8	13	1174 1177	51 51	1174 —	26·5 —	2	0·9
ω_8	e_{2g}	10	1	2		1584 1584·6	22·9 9·4	1584 1584·6	15·6 14	1	1·8

† Painter and Koenig (1977).
‡ Taddei *et al.* (1973).
§ Gee and Robinson (1967).
¶ Bonadeo *et al.* (1972).

(*b*) The most striking result concerns the effect of isotopic impurities (Trout *et al.* 1985). At natural abundance these lower the decay time by a factor of 1·9, 1·6, 2·3 and 28 for the ω_9, ω_1, ω_{10} and ω_6 modes, respectively. In the case of ω_8 the decay time for one factor group component decreases by a factor of 1·2 while for a second increases by a factor of 1·3. As discussed above, isotopic impurities can act as scattering or trapping centres, depending on whether they fall in the amalgamated or separated band limit. Their action greatly depends on the isotopic shift as compared to the vibron bandwidth. As can be seen from the data of table 5, there is no obvious correlation between the observed effects and the ratio of isotopic shift to vibron bandwidth. Isotopic impurities of a single type can act in a complicated manner since they: (i) may produce clusters of new energy levels due to different molecular orientations at each site; (ii) slightly shift the energy levels into which the vibron can decay; and (iii) relax the **k** selection rules acting as crystal defects. For these reasons it is not possible to envisage a single mechanism of action. The effect of isotopic impurities must be considered separately for each mode, taking into account the exact structure of the energy levels in the pure and natural crystals, information that is not fully available at present for complex systems like benzene.

(*c*) The measured decay times in the pure crystal at low temperature can be interpreted as lower limits to the population relaxation times. In the benzene crystal the most likely relaxation process involves decay into a lower lying vibrational mode with the emission of a lattice phonon. A useful guide to the interpretation of the experimental results comes from the work of Righini *et al.* (1983) who investigated the relaxation processes of the 991 cm^{-1} A_g mode and, using an intermolecular potential that included atom–atom and quadrupole–quadrupole interactions, calculated the decay time for the symmetrical exciton component. The calculated decay time of 47 ps is lower than the experimental value for the pure crystal by only a factor of 1·3. To the lowest order of perturbation the ω_1 mode can decay into the ω_{10} or the ω_{17} mode with emission of phonons of 10 and 130 cm^{-1}, respectively. These calculations show that the decay into the ω_{10} mode is highly preferential. This is not due to the value of the two-phonon density of states at the proper frequency but to the values of the third order coupling coefficients. In addition these calculations show that intraband scattering gives a negligible contribution in the present case. Generalization of these results implies that the decay of a vibrational exciton into other internal modes with phonon emission can be highly mode selective due to the strength of the anharmonic interaction which depends on the intermolecular potential. Thus correlations can not necessarily

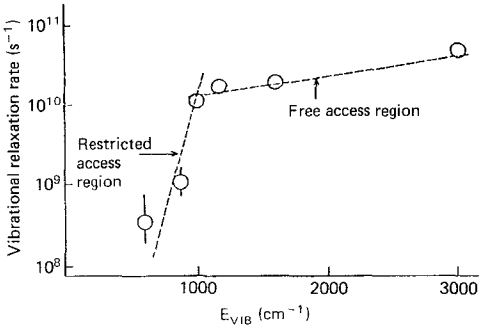

Figure 7. Vibrational relaxation rates of benzene vibrons as a function of excess vibrational energy. The dashed line is a visual guide.

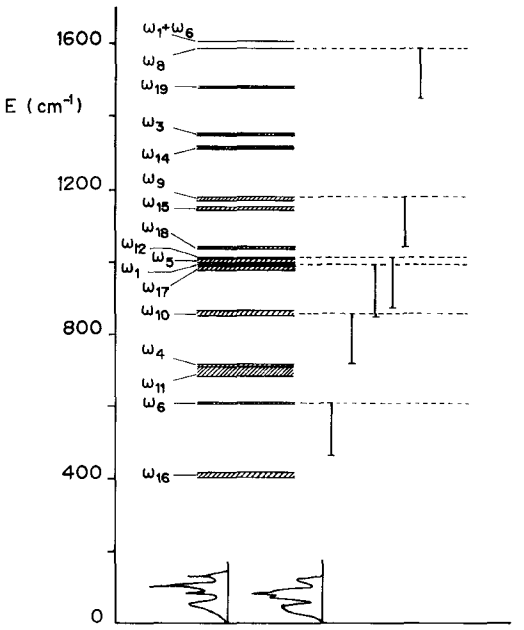

Figure 8. Energy level diagram for benzene vibrons. The diagrams at the bottom represent calculated lattice phonon densities of states. The length of vertical bars is equal to the lattice phonons band width.

be found between decay times and excess vibrational energy or number of available decay channels. These will occur in the case where all anharmonic coupling coefficients are equal in magnitude. Trout *et al.* (1985) were unable to find any correlation of the decay times with number of decay channels. The regular behaviour of the relaxation rate with respect to excess vibrational energy shown in figure 7 (Hochstrasser 1985) has thus been ascribed to increased anharmonicities of the benzene vibrations above $1000\,cm^{-1}$, such that 'restricted' and 'free' access regions can be distinguished below and above $1000\,cm^{-1}$, respectively. These conclusions were, however, reached starting from an incorrect phonon density of states. In fact, Trout *et al.* (1985) used a phonon density of states extending up to $250\,cm^{-1}$. This corresponds to the envelope of the inelastic neutron-scattering spectrum that includes an extended two-phonon tail (Bokhenkov *et al.* 1978). It is known from calculations (Bokhenkov *et al.* 1978) that the actual phonon density of states in benzene may extend up to $130–145\,cm^{-1}$, depending on the molecular geometry or intermolecular potential used. Using more appropriate phonon densities of states and considering down conversion processes of the lowest order we have re-evaluated the number of accepting modes and the 'relative' sums of weighted one-phonon channels discussed by Trout *et al.* (1985). The results are in table 5 and were obtained as an average for the two different calculated densities of states in figure 8. There is a reasonable correlation between number of available decay channels and measured decay times. A revised version of the energy levels diagram for excitons in crystalline benzene is shown in figure 8.

(*d*) In a few cases (ω_1, ω_9, ω_8) more than one factor group component has been observed in the high resolution CW CARS spectrum. As can be seen from table 5, these have different decay times. The A_g and B_{2g} factor group components of the ω_1 mode

have been studied in particular detail. In a time-resolved CARS experiment with appropriate geometry selection they were found to generate quantum beats (Velsko *et al.* 1983). They are separated by only 0·64 cm^{-1}. It is evident that if the decay is only due to population relaxation the same characteristic time is expected for the two components. In fact at such small frequency separation the same decay routes would be available for all components. It is still possible for the anharmonic coupling coefficients to be different for components of different symmetry. However, Trout *et al.* (1985) claim that the decay times differ not for the efficiency of the population relaxation mechanism but because of the contribution of dephasing mechanisms. This conclusion is suggested by the different position of the A_g and B_{2g} components within the exciton band. The A_g component is at the lower frequency edge of the vibron band where the density of states is approximately zero and then the defect scattering contribution (or defect and isotopic impurity scattering for the natural crystal) is negligible. On the contrary the B_{2g} component falls in a region where the density of states is appreciable. In this case the contribution of scattering processes is small but not negligible.

(*e*) The effect of added impurities on the decay time has been further investigated in mixed C_6H_6/C_6D_6 crystals, particularly for C_6D_6 concentrations up to 20% (Ho *et al.* 1983). In this range a monotonic shortening of the decay time for the 991 cm^{-1} mode has been found. The effect of added impurities can be very complicated. In the present case the isotopic impurity is in the separated band limit (with an isotopic frequency shift of 50 cm^{-1}). The impurity will then act as an additional trap for the vibron energy thus leading to the observed shortening of the decay time. In addition other impurity levels may also act as traps for the vibron energy. It is believed that the favourite trap is the impurity level corresponding to the same mode as the vibron investigated. Beside this, the trapping mechanisms in the mixed crystal can be of different types, and changing the concentration in a broader range may lead to changes in the mechanism of trapping (Velsko and Hochstrasser 1985 b). This may give rise to a non-monotonic behaviour of the decay time with impurity concentration. This is indeed observed for the 991 cm^{-1} mode in benzene as shown in figure 9.

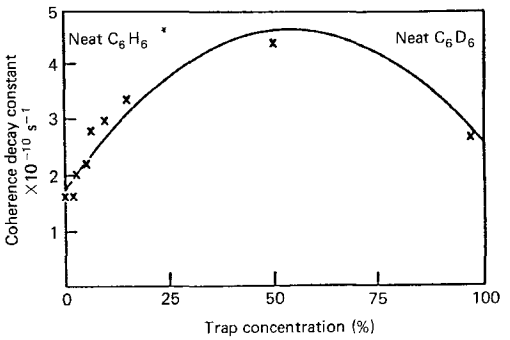

Figure 9. Variation of the relaxation rate constant of the ω_1 vibron of benzene in mixed C_6H_6/C_6D_6 crystals.

3.2.3. *Naphthalene*

The dynamics of naphthalene vibrons have been probed by various techniques including low (Bellows and Prasad 1979, Hess and Prasad 1980) and high-resolution spontaneous (Ranson *et al.* 1984), frequency (De Cola *et al.* 1980) and picosecond time resolved CARS (Hesp and Wiersma 1980, Dlott *et al.* 1982, Chronister and Dlott 1983,

Schosser and Dlott 1984, Chronister *et al.* 1985). Naphthalene is a system of considerable molecular complexity and, in order to extract useful information, investigations have been extended to normal and perdeutero compounds and their mixed crystals, to temperature dependence of the vibron decay times and to monodeutero naphthalenes. Objects of study have been several A_g molecular modes and one B_{3g} mode. A summary of the low-temperature decay times in Nh_8 and Nd_8 obtained by various workers is contained in table 6. It can be seen that, when allowance is made for the intrinsic uncertainty of these measurements, the various experiments are in reasonable agreement.

Attempts to recognize general trends in these data should be made with caution, in particular considering that the experiments refer to natural crystals and remembering that in benzene it was found that isotopic impurities at natural abundance can affect decay times considerably. At natural abundance the concentration of $^{13}C^{12}C_9H_8$ molecules amounts to 10% with the additional complication of three different positions for the ^{13}C impurity in a molecule. There is no apparent correlation of the decay times with excess vibrational energy. This is particularly evident looking at the ω_9 and ω_{17} modes that are only $3\,cm^{-1}$ apart and have quite different decay times. The mode dependence of the decay time is most clearly evidenced in the behaviour of the ω_{17} exciton. The two-factor group components of this mode are separated by only $0{\cdot}88\,cm^{-1}$ but their decay times differ by a factor of three. In an attempt to find a rationale for the observed decay times of naphthalene vibrons it was necessary to assume (Schosser and Dlott 1984, Chronister and Dlott 1983) that the average cubic anharmonic coefficients are characteristic of each mode and may differ from mode to mode by a factor of two or three. This has been confirmed in recent calculations by Righini (1984) of decay times of some of the naphthalene vibrons using model potentials, with the further circumstance that for each mode the decay into the underlying accepting modes is preferential. For instance, the $511\,cm^{-1}$ A_g mode can

Table 6. Vibrational relaxation times for internal modes of crystalline naphthalene and naphthalene-d_8 at 10 K.

		Naphthalene-h_8					Naphthalene-d_8			
			Decay times (ps)					Decay times (ps)		
		$\nu(cm^{-1})$	†	‡	§	¶	$\nu(cm^{-1})$	†	§	¶
ω_3	a_g	1578			14		1584		<10	
ω_5	a_g	1385	92	133	92	124	1390	<5	<10	
						118				
ω_6	a_g	1146			<10		863	<5	<10	
ω_7	a_g	1021	22		19		829		<10	
ω_8	a_g	766	78		62	89	701	<5	<10	
ω_9	a_g	514	140		128	152	493	74	50	76
						48				
ω_{17}	b_{3g}	511				33				

Hesp and Wiersma (1980).
‡ Decola *et al.* (1980).
§ Schosser and Dlott (1984).
¶ Ranson *et al.* (1984).

decay, with one phonon emission into ω_{47} (476 cm^{-1}), ω_{16} (468 cm^{-1}) and ω_{12} (392 cm^{-1}). Righini (1984) found that decay into ω_{16} contributes 59% of the linewidth of 0 K: this is partly due to the high density of two phonon states and partly to favourable values of the cubic anharmonic coefficients. He found reasonable agreement between observed and calculated decay times for ω_7, ω_8 and ω_9 while for ω_5 the calculated decay time is one order of magnitude larger than observed. The origin for this large discrepancy is not understood. The smallness of the coupling coefficients is ascribed by Righini (1984) to an inadequate description of the normal coordinate for this mode. It has been suggested (Schosser and Dlott 1984) that the decay of the naphthalene vibrons into two other internal modes (in near Fermi resonance) assisted by phonon emission could play an important role. Dlott assumed that these processes can lead to an intramolecular vibrational relaxation or to intermolecular decay arising from quartic anharmonicities and, by state counting, evaluated the number of two vibron states available at each frequency and found this number to increase rapidly with excess vibrational energy. As discussed in detail in the next paragraph, it is appropriate to assume that in these circumstances the vibrational relaxation is a mixed process involving cubic intra- and inter-molecular couplings. Since the intramolecular anharmonicity of importance is a one site property, and neglecting the effect of reduced molecular symmetry in the crystal, the two vibron states of interest for the decay of the totally symmetrical vibrons should be A_g molecular combination or overtone states. The number of available states is then 10, 6, 7, 5 and 2 for the ω_3, ω_5, ω_6, ω_7 and ω_8 vibrons, respectively. These numbers are much smaller than those reported by Schosser and Dlott (1984). To estimate the contribution of these processes would require knowledge of spectroscopic properties of the naphthalane molecule that is not available at present.

In perdeuteronaphthalene there is a general and pronounced shortening of the decay times (Schosser and Dlott 1984). Assuming that the magnitude of the anharmonic coupling coefficients does not change on deuteration, this behaviour can be well understood considering that the frequency shift of the vibrational states leads to an increase in density of acceptor states at each frequency. The same occurs to a more limited extent for monodeuterated naphthalenes (Chronister *et al.* 1985). For the latter, however, the reduction of molecular symmetry could also play an important role.

The linewidth of the a_g components of three of the naphthalene vibrons have been studied as a function of temperature between 0 K and the melting point. It is obvious that over such a wide temperature range the line broadening may be dominated in turn by various mechanisms. Below 40 K the linewidths reach a temperature-independent limit. The initial transient of the decay curves show some irregularities (Hesp and Wiersma 1980, Schosser and Dlott 1984) and, in the frequency domain, the a_g component at 766 cm^{-1} exhibits a high-frequency tail. Despite these features that remain unexplained, the low-temperature line shape is considered lorentzian and the broadening homogeneous. In this range there is a general consensus that the line broadening is due to vibrational relaxation into lower-lying vibrons. In the intermediate temperature range (40–150 K) the behaviour appears to be more complicated. From early measurements, Dlott *et al.* (1982) found that the linewidths could be fitted to an Arrhenius plot with a single activation energy. Later however, more refined measurements (Schosser and Dlott 1984) showed that on a semilog plot (logarithm of the excess linewidth versus $1/T$) the curves are slightly concave upward and that the linewidth is proportional to T^n, with n ranging from 2·0 to 2·4 for the three vibrons. Schosser and Dlott (1984) evaluated the contribution to the linewidth due to a

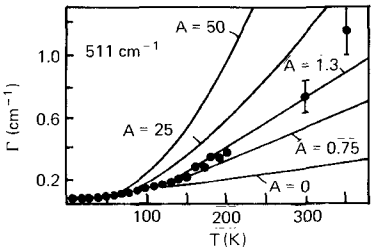

Figure 10. Experimental and calculated linewidth of a naphthalene vibron. Full lines are calculated curves (Schosser and Dlott 1984) with contribution of the energy exchange mechanism increasing with the value of A.

pure depopulation mechanism assuming that for each vibron the cubic coupling coefficient is constant and found (figure 10) that the predicted temperature dependence is gentler than observed. This is taken as evidence for the onset above 40 K of an additional thermally activated broadening mechanism which is identified with energy exchange (Harris *et al.* 1977) with low-frequency vibrons, which become appreciably populated with increasing temperature. It is possible to fit the experimental data as a result of the combined contribution of depopulation and exchange mechanism (see figure 10) but it is necessary to assume that the quartic anharmonic coefficients entering the latter are one order of magnitude larger than the cubic coefficients. However, it is the basic argument in favour of the onset of the energy exchange mechanism that is not well proved. In the calculations reported by Righini (1984) that consider only depopulation processes it is found that a good agreement can be obtained for the temperature dependence of the linewidth for the ω_7 mode, as can be seen from figure 11. Extrapolation of these calculations shows that the agreement is reasonably good even at 300 K. There is thus some evidence (e.g. the asymmetry of some of the bands and the curvature of the semilog plot) that down and up conversion processes are not the only contributors to the line broadening, but the other contributions have not been clearly identified.

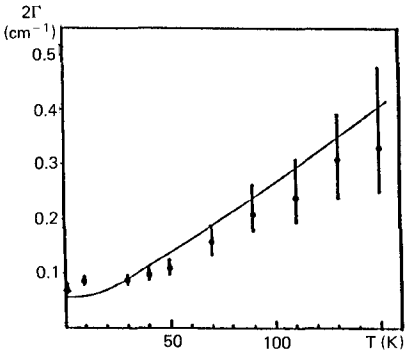

Figure 11. Temperature dependence of the 766 cm^{-1} vibron of naphthalene. The curve is calculated from Righini (1984).

At higher temperatures the line shape becomes more complex. The observed shape can be deconvoluted into homogeneous (lorentzian) and inhomogeneous (gaussian) contribution. The lorentzian linewidth can be discussed together with the homogeneous linewidth measured at lower temperatures. The inhomogeneous

linewidth is independent of temperature and is due to a slow modulation of the vibron frequency. It is thought that slow fluctuations of the density modulate the intermolecular potential and thus the vibron frequency. According to this model the high temperature solid resembles the liquid.

3.2.4. *Anthracene*

The lifetimes of some anthracene vibrons have been determined through time-resolved spectroscopy (Schosser and Dlott 1984) and the low-temperature data are summarized in table 7. It can be seen that lifetimes in anthracene are definitely shorter than in naphthalene and in general close to the instrumental limit. This shortening of the lifetime is due to the increasing density of vibron states and thus to the increasing number of acceptor states. Again, as discussed for naphthalene, there is no apparent correlation between the lifetimes and the excess vibrational energy.

Table 7. Vibrational relaxation times of internal modes of anthracene and anthracene-d_{10} at 10 K (in ps).

Anthracene		Anthracene-d_{10}	
$\nu(cm^{-1})$	T_2	$\nu(cm^{-1})$	T_2
1403	17	1388	<10
1261	15	1164	—
1163	21	842	<10
1008	<10	824	<10
753	35	707	18
395	53	382	<10

3.2.5. *Relaxation of two-phonon bound states*

The vibrational relaxation of internal modes in the overtone or combination region is particularly interesting in view of the peculiarity of the structure of the energy levels in this region. For a combination mode $\omega_1(\mathbf{k}_1)+\omega_2(\mathbf{k}_2)$ the wave vector conservation only concerns the total wave vector $\mathbf{k}_1+\mathbf{k}_2\simeq 0$ and thus the combination mode broadens into a band of width equal to the sum of the band widths of two vibrons (Dows and Schettino 1973). The width of the free two-phonon band is thus determined by the intermolecular interaction W. The intramolecular anharmonicity X may introduce additional features in the spectrum (Bogani 1978 a, b). The renormalized Green's function can have new poles inside (*resonances*) (Bogani 1978 b, Salvi and Schettino 1979, Righini *et al.* 1977) or outside (*bound states*) (Bogani 1978 b, Bogani *et al.* 1984, Bogani and Salvi 1984) the free two-phonon continuum. The structure of spectrum is determined by the relative magnitude of the intermolecular and anharmonic intramolecular couplings. When $X>W$, bound states may split off the continuum and appear in the spectrum as sharp peaks. It is evident that various situations may be encountered depending on the molecular system under investigation. In particular we may observe:

(*a*) sharp bound states on one side (generally at lower frequency) of a continuum;
(*b*) sharp bound states on both sides of a continuum;
(*c*) bound states at different separation from the continuum depending on the strength of the anharmonic interaction; and
(*d*) different widths of the continuum depending on the intermolecular coupling.

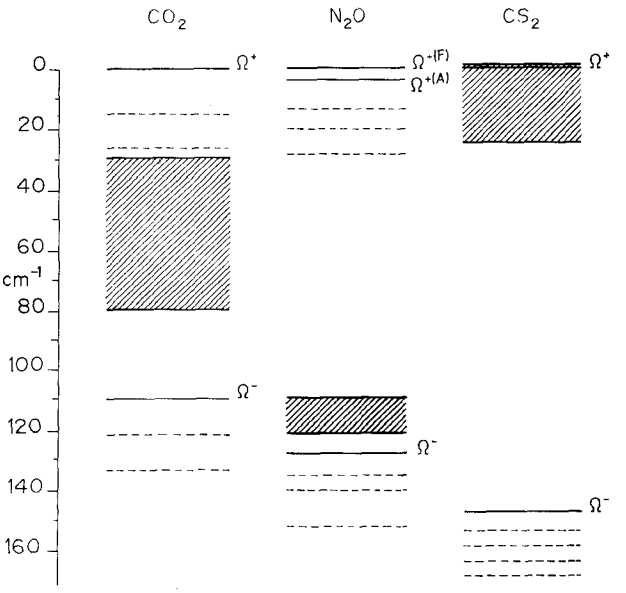

Figure 12. Energy level diagrams in the Fermi resonance region of some triatomic molecules. Dotted lines represent energy levels of isotopic impurities. The dashed region is the free two-phonon continuum.

This variety is particularly useful to investigate systematically the parameters governing the vibrational relaxation of the bound states. As an example, the energy spectrum in the $\omega_1, 2\omega_2$ Fermi resonance region is schematically represented in figure 12 for the CO_2 (Bogani and Salvi 1984), N_2O (Cardini *et al.* 1988) and CS_2 (Cardini *et al.* 1987) crystals that have been studied by coherent time resolved excitation (Geirnaert *et al.* 1984, Gale *et al.* 1984, Vallee *et al.* 1986, Ouillon and Ranson 1986) and by high-resolution Raman spectroscopy (Ranson *et al.* 1986, Ouillon *et al.* 1985). Because of the unit cell symmetry all the bound states are actually doublets of Davydov components: this is displayed only for the N_2O Ω^+ states where the two components are at larger separation ($5\,cm^{-1}$) as observed in the Raman spectrum at low resolution and reproduced in calculations in the dipole–dipole approximation (Cardini *et al.* 1988). The diagram also shows by dotted lines the position of the lines of major isotopic impurities that may play a role in the relaxation of the bound states acting as scattering or trapping centres. As can be seen from the figure, the structure of the energy bands is quite different in the three cases and this should lead to rather different dynamics of the bound states, in particular at lower temperatures. For CO_2 the behaviour at temperatures lower than 70 K has been studied in detail by high-resolution Raman spectroscopy. The use of polarized light has also allowed a separate study of the A_g and F_g components of the Davydov splitting. The results for the Ω^+ and Ω^- states are summarized in figure 13 and 14. The main points are the following: (*a*) the decay rate is definitely faster for the higher frequency Ω^+ states; (*b*) the decay is exponential, as shown by the lorentzian band shape, except for the Ω^- state at the lowest temperature; (*c*) the decay times for the A_g and F_g components of the bound states are different. These findings were simply rationalized by Ranson *et al.* (1986) assuming that the decay occurs by down (for the Ω^+ states) and up (for the Ω^- states) conversion into the free

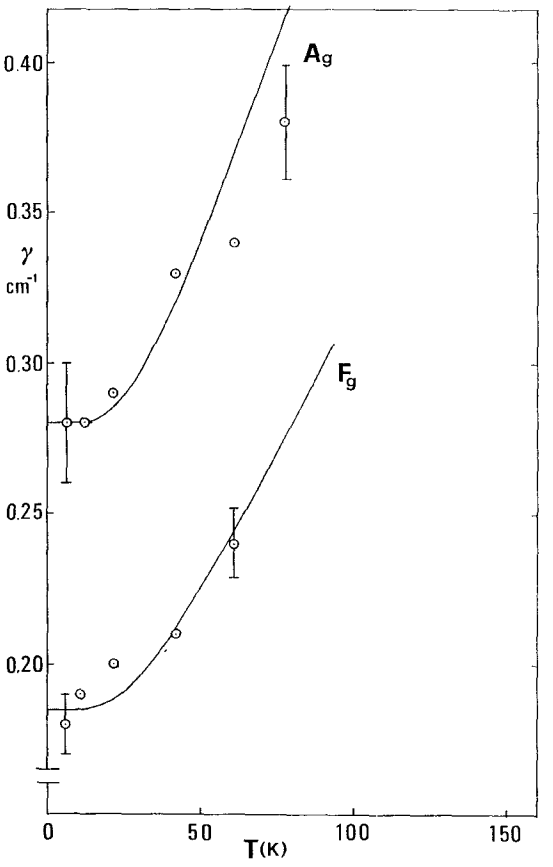

Figure 13. Temperature variation of the linewidth of the Ω^+ states in crystalline CO_2.

two-phonon continuum assisted by the absorption or emission of a lattice phonon according to diagrams 2 and 4 with $j=\Omega^+$ or Ω^-, j_1 and $j_2=\omega_2$. The temperature behaviour will then be governed by expressions (15) and (17). In the present case the occupation numbers for the internal modes can be approximated as zero. Therefore in the limit of constant coupling coefficients we have for the temperature-dependent bandwidths

$$\left.\begin{aligned}\Gamma^+(T)&=\Gamma^+(0)[1+n_1]\\ \Gamma^-(T)&=\Gamma^-(0)+Cn_1\end{aligned}\right\} \tag{32}$$

The observed temperature behaviour is satisfactorily reproduced by processes assisted by a $60\,cm^{-1}$ lattice phonon as shown in figures 13 and 14. This is reasonable, considering that the phonon density of states is actually peaked at approximately $60\,cm^{-1}$.

However, this approach oversimplifies the problem and offers two major difficulties. The bound state is a complicated admixture of all the states of the continuum and it is not possible to find a simple form of the coordinate describing it. It will thus not be easy to estimate the coupling coefficients governing the line broadening according to the above diagrams. Secondly, the intramolecular anharmonicity that plays a dominant role in the formation of the bound states does not enter explicitly in

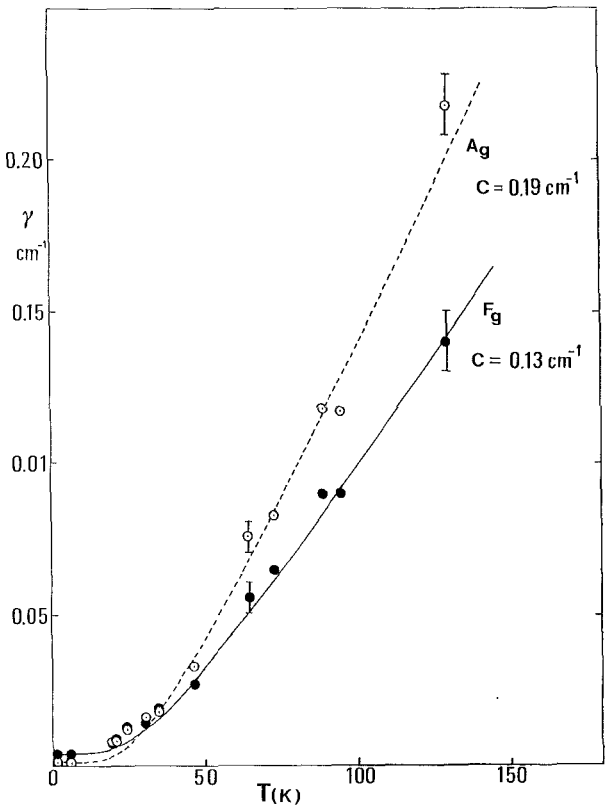

Figure 14. Temperature variation of the linewidth of the Ω^- states in crystalline CO_2.

the relaxation process. A more satisfactory theory of the relaxation of two-phonon bound states and resonances has been discussed recently (Bogani *et al.* 1988) starting from the assumption that there are two perturbations to the harmonic hamiltonian, the intramolecular anharmonicity and the coupling of internal modes to the lattice phonons, to be treated simultaneously. For the Fermi resonance between a fundamental ω_1 and an overtone $2\omega_2$, the Hamiltonian can be written as

$$H = H_0 + H_1 + H_3 + H_4 \tag{33}$$

with

$$\begin{aligned} H_0 &= \sum_{kjh} [\omega_1(k) Q_1^+(k) Q_1^-(k) + \omega_2(k) Q_2^+(k) Q_2^-(k) \\ &\quad + \omega_j(k) q_j^+(k) q_j^-(k)] \\ H_1 &= \sum_{k_1 k_2 k_3} K_{122} Q_1(k_1) Q_2(k_2) Q_2(k_3) \Delta(k_1 + k_2 + k_3) \\ H_3 &= \sum_{k_1 k_2 j k_3} [V^3(k_1 k_2 j k_3) Q_2(k_1) Q_2(k_2) q(j k_3) \\ &\quad + V^3(k_1 k_2 j k_3) Q_1(k_1) Q_1(k_2) q(j k_3)] \\ H_4 &= \sum_{k_1 k_2 i k_3 j k_4} [V^4(k_1 k_2 i k_3 j k_4) Q_2(k_1) Q_2(k_2) q(i k_3) q(j k_4) \\ &\quad + V^4(k_1 k_2 i k_3 j k_4) Q_1(k_1) Q_1(k_2) q(i k_3) q(j k_4)] \end{aligned} \tag{34}$$

where Q and q are internal and phonon coordinates, respectively, Q^+, Q^-, q^+ and q^- are appropriate creation and annihilation operators and i and j are phonon branch indices. Without loss of generality a single occupancy of the unit cell has been assumed. The H_1 term renormalizes the two phonon Green's function through the basic diagram

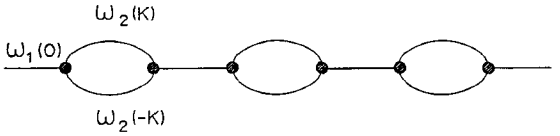

and may give rise in the spectrum to bound states of infinite lifetime. The cubic and quartic terms H_3 and H_4 shorten the lifetime of the bound state. The cubic terms lead to a relaxation of the bound state into the continuum with emission or absorption of a lattice phonon. This is in essence the same relaxation process considered by Ranson *et al.* (1986) but the diagrams describing it are quite different and can be represented as follows.

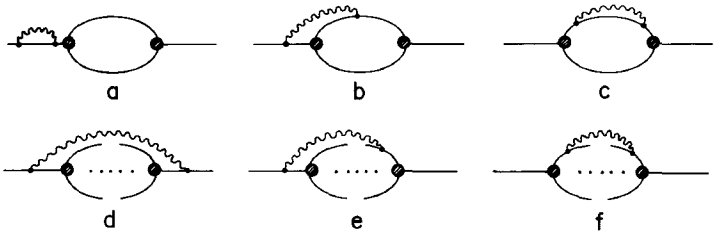

The diagrams in the first row are also effective for an isolated phonon line (for instance diagrams (*a*) and (*c*) describe intraband scattering and the origin of phonon side bands) while the diagram of the second row are specific to bound states. The quartic terms give rise to desphasing processes. Those involving the fundamental mode ω_1 may be described by diagrams that in a contracted form are of the following type.

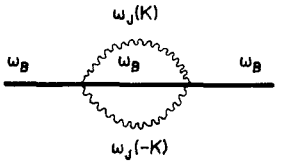

However, they actually appear in the following form.

Calculations of the bound state linewidth according to this theory have been carried out for a linear molecular crystal. The calculations show that the linewidth depends very much on the separation of the bound state from the edge of the continuum and thus on the ratio X/W. The shape of the free two-phonon continuum is also important. It has also been found that even at low temperature, and depending on the ratio X/W, the dephasing contribution can be as important as the relaxation process. The low-temperature residual linewidth is correctly predicted by the model and in particular the low-temperature behaviour of the Ω^- state is in good agreement with experimental results in crystalline CO_2 (Ouillon and Ranson 1986).

For the N_2O bound states the decay time has been measured by time-resolved picosecond techniques between 70 and 150 K (Valee *et al.* 1986). The decay has been found to be non-exponential at all temperatures. It has been ascribed to interference between the two Davydov components of the bound states and estimates of the A and F symmetry states decay times obtained. This interpretation could easily be verified by high-resolution Raman studies. A remarkable finding in N_2O is that the decay time for the Ω^+ and Ω^- states is slowly temperature dependent. We suggest the following explanation for this result. Down conversion of the states into the two phonon continuum may occur with the emission of a $120\,cm^{-1}$ phonon. In previous calculations of the intensity of phonon side bands in crystalline OCS (Della Valle *et al.* 1979 b) it has been found that coupling coefficients of the type V_{iil} (where i is an internal and l an external phonon) become very small at high-phonon energies. This is reflected in the vanishing of the phonon side bands at large separation from the fundamental. It is reasonable to assume that the same occurs in the N_2O crystal. In fact the intensity of the phonon side band accompanying the Ω^+ peak in the Raman spectrum becomes very small at frequencies higher than $120\,cm^{-1}$. The vanishing of the cubic coupling coefficients will make the down conversion processes not very effective and the decay could then be dominated by scattering or trapping at the isotopic impurity centre. This would lead to temperature-independent decay. On the other hand, the up-conversion processes for the Ω^- states would be assisted by absorption of acoustic phonons in the range $10–20\,cm^{-1}$. Since the coupling with acoustic phonons is again very small, in this case the relaxation could also be dominated by temperature-independent scattering or trapping by impurity centres. This could explain why the decay rates for the Ω^+ and Ω^- states in N_2O are quite similar.

In the case of the CS_2 crystal only the decay time for the Ω^+ state at a temperature close to the melting point has been measured. The situation is quite different from that encountered for CO_2 and N_2O. In fact the Ω^+ state in CS_2 falls within the continuum close to the edge, and is thus not strictly a bound state. For resonances there is a straightforward relaxation route into the continuum. The linewidth is directly proportional to the density of states and it will in general be large and approximately temperature independent. When, however, the resonance falls in regions of vanishing density of states the linewidth can be quite small. This is indeed the case for the Ω^+ state in CS_2. It would be interesting to investigate the temperature dependence of the linewidth of this state. Compared with the CO_2 case, the behaviour of the Ω^- state in CS_2 should also be distinctly different. In fact the limiting frequency in the CS_2 phonon density of states is at $110\,cm^{-1}$ (Burgos and Righini 1983) and therefore up-conversion processes assisted by absorption of a single phonon are not possible. The lowest order decay processes are then up conversion processes into the two-phonon continuum with absorption of two lattice phonons or down-conversion processes into the fundamental band with emission of three lattice phonons. It is possible that in this case a major role in the decay process is played by isotopic impurities, particularly in view of the high natural abundance of $^{12}C^{34}S^{32}S$. This would give rise to a temperature-independent decay route.

References

ABRAM, I. I., HOCHSTRASSER, R. M., KOHL, J. E., SEMACK, M. G., and WHITE, D., 1977, *Chem. Phys. Lett.*, **52**, 1.

ABRAM, I. I., HOCHSTRASSER, R. M., KOHL, J. E., SEMACK, M. G., and WHITE, D., 1979, *Chem. Phys. Lett.*, **71**, 153.

ABRAM, I. I., HOCHSTRASSER, R. M., KOHL, J. E., SEMACK, M. G., and WHITE, D., 1980, *Chem. Phys. Lett.*, **71,** 405.
ABRAM, I. I., and HOCHSTRASSER, R. M., 1980, *J. chem. Phys.*, **72,** 3617.
ANDERSON, A., and LEROI, G. E., 1966, *J. chem. Phys.*, **45,** 4359.
ANTRYGINA, T. N., SLUSONEV, V. A., FREIMAN, YU. A., and EREMBUG, A. J., 1984, *J. low temp. Phys.*, **56,** 331.
BELLOWS, J. C., and PRASAD, P. N., 1979, *J. chem. Phys.*, **70,** 1864.
BERNS, R. M., and VAN DER AVOIRD, A., 1980, *J. chem. Phys.*, **72,** 6107.
BOGANI, F., 1978 a, *J. Phys. C*, **11,** 1283.
BOGANI, F., 1978 b, *J. Phys. C*, **11,** 1297.
BOGANI, F., GIUIA, R., and SCHETTINO, V., 1984, *Chem. Phys.*, **88,** 375.
BOGANI, F., and SALVI, P. R., 1984, *J. chem. Phys.*, **81,** 4991.
BOGANI, F., CARDINI, G., SCHETTINO, V., and TASSELLI, P. L., 1988 (in the press).
BOKHENKOV, E. L., FEDOTOV, V. G., SHEKA, E. F., NATKANIEC, I., SUKNIK-HRYNLIEWICZ, M., CALIFANO, S., and RIGHINI, R., 1978, *Nuovo Cimento*, **44,** 324.
BONADEO, H., MARZOCCHI, M. P., CASTELLUCCI, E. M., and CALIFANO, S., 1972, *J. chem. Phys.*, **57,** 4299.
BONADEO, H., and BURGOS, E., 1985, *J. chim. Phys.*, **82,** 91.
BRIELS, W. J., JANSEN, A. P. J., and VAN DER AVOIRD, A., 1984, *J. chem. Phys.*, **81,** 4118.
BRIELS, W. J., JANSEN, A. P. J., and VAN DER AVOIRD, A., 1985, *J. chim. Phys.*, **82,** 125.
BROOKEMAN, J. R., CANEPA, P. C., MCEHNAN, M. M., and SCOTT, T. A., 1970, *Phys. Lett.*, **31A,** 04.
BROOKEMAN, J. R., MCEHNAN, M. M., and SCOTT, T. A., 1971, *Phys. Rev.* B, **4,** 366.
BURGOS, E., and RIGHINI, R., 1983, *Chem. Phys. Lett.*, **96,** 584.
CALAWAY, W. F., and EWING, G. E., 1975, *J. chem. Phys.*, **63,** 2842.
CALIFANO, S., SCHETTINO, V., and NETO, N., 1981, *Lattice Dynamics of Molecular Crystals.* Lecture Notes in Chemistry, Vol. 26 (Berlin: Springer).
CARDINI, G., and O'SHEA, S. F., 1985, *Phys. Rev.* B, **32,** 2489.
CARDINI, G., SALVI, P. R., and SCHETTINO, V., 1987, *Chem. Phys.*, **117,** 341.
CARDINI, G., SALVI, P. R., and SCHETTINO, V., 1988, *Chem. Phys.*, **119,** 241.
CHRONISTER, E. L., and DLOTT, D. D., 1983, *J. chem. Phys.*, **79,** 5286.
CHRONISTER, E. L., HILL, J. R., and DLOTT, D. D., 1985, *J. chim. Phys.*, **82,** 159.
COWLEY, R. A., 1963, *Adv. Phys.*, **12,** 421.
COWLEY, R. A., 1965, *Phil. Mag.*, **11,** 673.
DECOLA, P. L., HOCHSTRASSER, R. M., and TROMSDORFF, H. P., 1980, *Chem. Phys. Lett.*, **72,** 1.
DELALANDE, G., and GALE, G. M., 1977, *Chem. Phys. Lett.*, **50,** 339.
DELLA VALLE, R. G., FRACASSI, P. F., RIGHINI, R., CALIFANO, S., and WALMSLEY, S. H., 1979, *Chem. Phys.*, **44,** 189.
DELLA VALLE, R. G., FRACASSI, P. F., SCHETTINO, V., and CALIFANO, S., 1979, *Chem. Phys.*, **43,** 385.
DELLA VALLE, R. G., FRACASSI, P. F., RIGHINI, R., and CALIFANO, S., 1983, *Chem. Phys.*, **74,** 179.
DE SILVESTRI, S., FUJIMOTO, J. G., IPPEN, E. P., GAMBLE, JR, E. B., WILLIAMS, L. R., and NELSON, K. A., 1985, *Chem. Phys. Lett.*, **116,** 146.
DLOTT, D. D., 1986, *Ann. Rev. phys. Chem.*, **37,** 157.
DLOTT, D. D., SCHOSSER, C. L., and CHRONISTER, E. L., 1982, *Chem. Phys. Lett.*, **90,** 386.
DORNER, B., BOKLENKOV, E. L., CHAPLOT, S. L., KALUS, J., NATKANIEC, I., PAWLEY, G. S., SCHMELZER, V., and SHEKA, E. F., 1982, *J. Phys.* C, **15,** 2353.
DOWS, D. A., and SCHETTINO, V., 1973, *J. chem. Phys.*, **58,** 5009.
DUPPEN, K., HESP, B. M. M., and WIERSMA, D. A., 1981, *Chem. Phys. Lett.*, **79,** 399.
ELLIOTT, R. J., KRUMHANSL, J. A., and LEATH, P. L., 1974, *Rev. mod. Phys.*, **46,** 465.
ELLIOTT, R. J., 1975, in *Lattice Dynamics and Intermolecular Forces*, Proceedings of the LV International School of Physics (New York: Academic Press).
GALE, G. M., GUYOT-SIONNET, P., ZHENG, W. Q., and FLYTZANIS, C., 1984, *Phys. Rev. Lett.*, **54,** 825.
GEE, A. R., and ROBINSON, G. W., 1967, *J. chem. Phys.*, **46,** 4847.
GEIRNAERT, M. L., GALE, G. M., and FLYTZANIS, C., 1985, *Phys. Rev. Lett.*, **52,** 815.
HARRIS, C. B., SHELBY, R. M., and CORNELIUS, P. A., 1977, *Phys. Rev. Lett.*, **38,** 1415.
HESP, B. H., and WIERSMA, D. A., 1980, *Chem. Phys. Lett.*, **75,** 423.
HESS, L. H., and PRASAD, P. N., 1980, *J. chem. Phys.*, **72,** 573.
HO, F., TSAY, W. S., TROUT, J., and HOCHSTRASSER, R. M., 1981, *Chem. Phys. Lett.*, **83,** 5.

HO, F., TSAY, W. S., TROUT, J., and HOCHSTRASSER, R. M., 1983, *Chem. Phys. Lett.*, **97,** 141.
HOCHSTRASSER, R. M., 1985, in *Time Resolved Vibrational Spectroscopy*, edited by M. Stockburger and A. Lauberau (Berlin: Springer).
IVANOV, M. A., KVASHNINA, L. B., and KRIVOGLAZ, M. A., 1966, *Sov. Phys. Solid State*, **7,** 1652.
JANSEN, A. B. J., BRIELS, N. J., and VAN DER AVOIRD, A., 1984, *J. chem. Phys.*, **81,** 3648.
JINDAL, V. K., and KALUS, J., 1983, *J. Phys. C: Solid State Phys.*, **16,** 3061.
KALUS, J., 1985, *J. chim. Phys.*, **82,** 137.
KJEMS, J. K., and DOLLING, G., 1975, *Phys. Rev.* B, **11,** 1639.
KLAFTER, J., and JORTNER, J., 1978, *J. chem. Phys.*, **68,** 1513.
KOBASHI, K., 1978, *Mol. Phys.*, **36,** 225.
KOSIK, T. J., CLINE, Jr, R. E., and DLOTT, D. D., 1983, *Chem. Phys. Lett.*, **103,** 109.
KOSIK, T. J., CLINE, JR, R. E., and DLOTT, D. D., 1984, *J. chem. Phys.*, **81,** 4932.
LAUBERAU, A., and KAISER, W., 1978, *Rev. Mod. Phys.*, **50,** 607.
MURTHY, C. S., O'SHEA, S. F., and MCDONALD, I. R., 1983, *Mol. Phys.*, **50,** 531.
MARADUDIN, A. A., 1968, *Solid State Phys.*, **19,** 1.
NATKANIEC, I., BOKHENKOV, E. L., DORNER, B., KALUS, J., MACKENZIE, G. A., PAWLEY, G. S., SCHMELZER, U., and SHEKA, E. F., 1980, *J. Phys.* C, **13,** 4265.
OUILLON, R., RANSON, P., and CALIFANO, S., 1984, *Chem. Phys.*, **91,** 119.
OUILLON, R., RANSON, P., and CALIFANO, S., 1984, *Proceedings of the IXth International Raman Conference*, Tokyo, p. 202.
OUILLON, R., RANSON, P., and CALIFANO, S., 1985, *J. chem. Phys.*, **83,** 2162.
OUILLON, R., and RANSON, P., 1986, *J. chem. Phys.*, **85,** 1295.
PAINTER, P., and KOENIG, J. L., 1977, *Spectrochim. Acta*, **33A,** 1003.
PERRIN, B., 1987, private communication.
PRASAD, P. N., and VON SMITH, R., 1979, *J. chem. Phys*, **71,** 4646.
PROCACCI, P., RIGHINI, R., and CALIFANO, S., 1987, *Chem. Phys.*, **116,** 171.
RAICH, J. C., GILLS, N. S., and ANDERSON, A. B., 1974, *J. chem. Phys.*, **61,** 9399.
RANSON, P., OUILLON, R., and CALIFANO, S., 1984, *Chem. Phys.*, **86,** 115.
RANSON, P., OUILLON, R., HALAC, B., and CALIFANO, S., 1985, *J. chim. Phys.*, **82,** 169.
RANSON, P., OUILLON, R., and CALIFANO, S., 1986, *J. Raman Spectrosc.*, **17,** 155.
RANSON, P., OUILLON, R., and CALIFANO, S., 1988, *J. Chem. Phys.* (in the press).
RIGHINI, R., FRACASSI, P. F., and DELLA VALLE, R. G., 1983, *Chem. Phys. Lett.*, **97,** 308.
RIGHINI, R., 1984, *Chem. Phys.*, **84,** 97.
RIGHINI, R., SALVI, P. R., and SCHETTINO, V., 1977, *Mol. Cryst. liq. Cryst.*, **43,** 223.
RON, A., and SHNEPP, O., 1967, *J. chem. Phys.*, **46,** 3991.
SALVI, P. R., and SCHETTINO, V., 1979, *Chem. Phys.*, **40,** 413.
SCHMIDT, J. W., and DANIELS, W. B., 1980, *J. chem. Phys.*, **73,** 4848.
SCHOSSET, C. L., and DLOTT, D. D., 1984, *J. chem. Phys.*, **80,** 1394.
SIGNORINI, G. F., FRACASSI, P. F., RIGHINI, R., and DELLA VALLE, G. G., 1985, *Chem. Phys.*, **100,** 315.
ST LOUIS, R. V., and SCHNEPP, O., 1969, *J. chem. Phys.*, **50,** 5177.
TADDEI, G., BONADEO, H., MARZOCCHI, M. P., and CALIFANO, S., 1973, *J. chem. Phys.*, **58,** 966.
TRIPATHI, R. S., and PATHAK, K. N., 1974, *Nuovo Cimento*, **21B,** 289.
TROUT, J., VELSKO, S., BOZIO, R., DECOLA, P. L., and HOCHSTRASSER, R. M., 1985, *J. chem. Phys.*, **81,** 4746.
VALLEE, F., GALE, G. M., and FLYTZANIS, C., 1986, *Chem. Phys. Lett.*, **124,** 216.
VAN DER AVOIRD, A., BRIELS, W. J., and JANSEN, A. P. J., 1984, *J. chem. Phys.*, **81,** 3685.
VELSKO, S., TROUT, J., and HOCHSTRASSER, R. M., 1983, *J. chem. Phys.*, **79,** 2114.
VELSKO, S., and HOCHSTRASSER, R. M., 1985 a, *J. phys. Chem.*, **89,** 2240.
VELSKO, S., and HOCHSTRASSER, R. M., 1985 b, *J. chem. Phys.*, **82,** 2180.
WALMSLEY, S. H., 1985, *J. chim. Phys.*, **82,** 117.
WALMSLEY, S. H., 1986, *Int. Rev. phys. Chem.*, **5,** 185.